Fbxw7 increases CCL2/7 in CX3CR1^{hi} macrophages to promote intestinal inflammation

Jia He, … , Lihua Lai, Qingqing Wang

Research Article **Immunology** **Inflammation**

Resident and inflammatory mononuclear phagocytes (MPhs) with functional plasticity in the intestine are critically involved in the pathology of inflammatory bowel diseases (IBDs), the mechanism of which remains incompletely understood. In the present study, we found that increased expression of the E3 ligase F-box and WD repeat domain–containing 7 (FBXW) in the inflamed intestine was significantly correlated with IBD severity in both human diseases and in mouse models. Myeloid *Fbxw7* deficiency protected mice from colitis induced by dextran sodium sulfate (DSS) or 2,6,4-trinitrobenzene sulfonic acid (TNBS). *Fbxw7* deficiency resulted in decreased production of the chemokines CCL2 and CCL7 by colonic CX3CR1^{hi} resident macrophages and reduced the accumulation of CX3CR1^{int} proinflammatory MPhs in colitis-affected colon tissue. Mice that received adeno-associated virus–shFbxw7 (AAV-shFbxw7) showed significantly improved survival rates and alleviation of colitis. Mechanism screening demonstrated that FBXW7 suppressed H3K27me3 modification and promoted *Ccl2* and *Ccl7* expression via degradation of the histone-lysine*N*-methyltransferase enhancer of zeste homolog 2 (EZH2) in macrophages. Taken together, our results indicate that FBXW7 degrades EZH2 and increases *Ccl2* and *Ccl7* in CX3CR1^{hi} macrophages, thereby promoting the recruitment of CX3CR1^{int} proinflammatory MPhs into local colon tissues with colitis. Targeting FBXW7 might represent a potential therapeutic approach for the treatment of intestinal inflammation.

Find the latest version:

https://jci.me/123374/pdf

Fbxw7 increases CCL2/7 in CX3CR1hi macrophages to promote intestinal inflammation

Jia He,[1] Yinjing Song,[1] Gaopeng Li,[1] Peng Xiao,[2] Yang Liu,[1] Yue Xue,[1] Qian Cao,[2] Xintao Tu,[1] Ting Pan,[1] Zhinong Jiang,[3] Xuetao Cao,[1,4] Lihua Lai,[1] and Qingqing Wang[1]

[1]Institute of Immunology, Zhejiang University School of Medicine, Hangzhou, Zhejiang, China. [2]Department of Gastroenterology and [3]Department of Pathology, Sir Run Run Shaw Hospital, Zhejiang University School of Medicine, Hangzhou, Zhejiang, China. [4]National Key Laboratory of Medical Molecular Biology, Institute of Basic Medical Sciences, Peking Union Medical College, Chinese Academy of Medical Sciences, Beijing, China.

Resident and inflammatory mononuclear phagocytes (MPhs) with functional plasticity in the intestine are critically involved in the pathology of inflammatory bowel diseases (IBDs), the mechanism of which remains incompletely understood. In the present study, we found that increased expression of the E3 ligase F-box and WD repeat domain–containing 7 (FBXW) in the inflamed intestine was significantly correlated with IBD severity in both human diseases and in mouse models. Myeloid *Fbxw7* deficiency protected mice from colitis induced by dextran sodium sulfate (DSS) or 2,6,4-trinitrobenzene sulfonic acid (TNBS). *Fbxw7* deficiency resulted in decreased production of the chemokines CCL2 and CCL7 by colonic CX3CR1hi resident macrophages and reduced the accumulation of CX3CR1int proinflammatory MPhs in colitis-affected colon tissue. Mice that received adeno-associated virus–shFbxw7 (AAV-shFbxw7) showed significantly improved survival rates and alleviation of colitis. Mechanism screening demonstrated that FBXW7 suppressed H3K27me3 modification and promoted *Ccl2* and *Ccl7* expression via degradation of the histone-lysine *N*-methyltransferase enhancer of zeste homolog 2 (EZH2) in macrophages. Taken together, our results indicate that FBXW7 degrades EZH2 and increases *Ccl2* and *Ccl7* in CX3CR1hi macrophages, thereby promoting the recruitment of CX3CR1int proinflammatory MPhs into local colon tissues with colitis. Targeting FBXW7 might represent a potential therapeutic approach for the treatment of intestinal inflammation.

Introduction

Chronic and progressive inflammation is the key pathogenesis of inflammatory bowel disease (IBD) including Crohn's disease (CD) and ulcerative colitis (UC), which involve dysregulation of the genetic, environmental, or microbial factors and immune responses. A macrophage-induced innate immune response within the intestinal mucosa is the first line of defense against the invading pathogens (1–3). Inefficient or overactivation of gastrointestinal macrophage subsets participate in IBD development by regulating the initiation, amplification, and resolution of local inflammation (4–6).

Monocyte-derived mononuclear phagocytes (MPhs) in colonic lamina propria (CLP) express certain levels of the chemokine CX3C receptor CX3CR1 and CD11b (7, 8). In a healthy colon, Ly6Chi (Ly6C high-positive) monocytes mainly give rise to CX3CR1hi (CX3CR1 high-positive) resident macrophages that contribute to the maintenance of gut homeostasis and protect the host from certain pathogens (9, 10). However, the phenotype and fate of mucosal monocyte–derived MPhs change dramatically in inflammatory environments. Under these circumstances, CX3CR1hi resident macrophages that dominate in the healthy colon are replaced by

inflammation-elicited plastic CX3CR1int (CX3CR1 intermediate-positive) MPhs that are the progeny of rapidly infiltrating Ly6Chi circulating peripheral blood monocytes (11), which express higher levels of proinflammatory mediators and TLRs, NO, reactive oxygen intermediates, cathepsins, and metalloproteases than do their resident counterparts, forming an intense infiltration into CLP. As a result, CX3CR1int proinflammatory MPhs aggravate the intestinal inflammatory response and play crucial roles in the pathogenesis of CD and UC (7). Although the cells in this MPh pool are on a differentiation waterfall that may include cell populations that have predominantly more macrophage-like functions, there are also a small number of cells with DC-like functions (10). Therefore, herein, we refer to CLP CX3CR1int macrophages as CX3CR1int MPhs.

The infiltration of CX3CR1int proinflammatory MPhs can be triggered by dysregulated expression of chemokines in inflamed colon tissues through recruitment of Ly6Chi monocytes, which differentiate into CX3CR1int proinflammatory MPhs and produce proinflammatory cytokines including IL-6 and TNF-α (12, 13). Chemokines are produced by a wide variety of cells, including the inflammatory cells present in IBD lesions, fibroblasts, and endothelial and epithelial cells in the gastrointestinal system. The potent capacity of macrophages to secrete chemokines to mediate immune cell recruitment is critical for the inflammation cascade and has been demonstrated in previous studies (14–16). It has been reported that the increase of inflammatory macrophages in patients with IBD who do not respond to anti–TNF-α therapy is associated with an upregulation of the TREM-1/CCL7/ CCR2 axis (17). The induction of chemokines has been reported to

occur via activation of the NF-κB signaling cascade (18–20), however, mechanisms by which the complex cytokine and chemokine network in the colonic microenvironment influences inflammatory MPh infiltration are not well defined and represent a fundamental gap in the understanding of homeostatic immune function and IBD development.

F-box and WD repeat domain–containing 7 (FBXW7) is a component of the SKP1, CUL1, and F-box protein type ubiquitin ligase (SCF) complex. *Fbxw7* mutations have been identified in various types of cancers (21). FBXW7 is also reported to regulate lipid metabolism (22), target osteogenic and chondrogenic transcriptional factors (23), interact with parkin, and play important roles in Parkinson's disease (24). Our previous study showed that FBXW7 is critical for promoting innate antiviral immunity by mediating the ubiquitination of SHP2 (25). However, the function and mechanisms of FBXW7 in inflammation responses have not been clarified. In this study, we found that FBXW7 expression was markedly increased in inflamed intestinal tissues from patients with UC or CD. *Fbxw7* deficiency in myeloid cells reduced inflammation and disease severity in the colitis mouse model. FBXW7 promoted enhancer of zeste homolog 2 (EZH2) ubiquitination and decreased the modification of H3K27me3 on the promoters of the chemokines *Ccl2* and *Ccl7*. We found that the FBXW7/EZH2/CCL2/CCL7 pathway heightened the severity of colitis through recruitment of CX3CR1^{int} proinflammatory MPhs, and propose that FBXW7 may serve as a new diagnostic marker.

Results

Increased FBXW7 expression in IBD. We first analyzed the expression levels of *FBXW7* in colonic mucosa samples, with or without signs of inflammation, from patients with UC in the Gene Expression Omnibus (GEO) database. Compared with healthy mucosa, *FBXW7* expression was significantly increased in active UC mucosa, but less so in inactive UC mucosa (Supplemental Figure 1A; supplemental material available online with this article; https://doi.org/10.1172/JCI123374DS1). Moreover, the expression of FBXW7 in colon tissue macrophages observed by immunohistochemical and immunofluorescence staining (Figure 1, A and B) and mRNA expression of *FBXW7* in peripheral blood monocytes (Figure 1C) were markedly increased in patients with IBD compared with healthy control subjects or non–IBD inflammation (acute diarrhea) control (ICs). *FBXW7* mRNA levels in peripheral blood monocytes was significantly higher in patients with UC (Supplemental Figure 1B) or CD (Supplemental Figure 1C), who had severe colitis, than in those with mild colitis or in healthy controls. However, we detected no difference in *FBXW7* expression levels in peripheral blood lymphocytes from patients with IBD and control subjects (Figure 1D).

The expression of FBXW7 in CD11b$^+$CX3CR1$^+$ CLP macrophages (Figure 2, A and B) was significantly increased in the dextran sodium sulfate–induced (DSS-induced) colitis mouse model and in *Il10* gene–KO (*ll10$^{-/-}$*) mice, and *Fbxw7* mRNA expression in peripheral blood monocytes of mice (Figure 2C) showed a progressive increase upon DSS challenge. FBXW7 expression in Ly6C^{hi} colonic monocytes was also dramatically increased (Figure 2D). Moreover, immunofluorescence staining confirmed an upregulation of FBXW7 expression in colonic CD68$^+$ macrophages (Figure

2E) and F4/80$^+$ macrophages (Figure 2F) after DSS treatment for 5 days compared with expression in the colons of healthy mice. These results suggest that increased FBXW7 expression in monocytes and macrophages was correlated with local colonic inflammation in both humans and mice.

Fbxw7 deficiency attenuates experimental colitis. To investigate the role of *Fbxw7* in macrophages in colitis, LysM-Cre$^+$ *Fbxw7$^{fl/fl}$* (*LysM$^+$ Fbxw7$^{fl/fl}$*) mice and their control littermates (*Fbxw7$^{fl/fl}$*) were subjected to acute colitis induction using 3% DSS. Colitis-induced macroscopic changes (body weight loss, diarrhea, and rectal bleeding) were significantly alleviated in the *LysM$^+$ Fbxw7$^{fl/fl}$* mice compared with *Fbxw7$^{fl/fl}$* littermates (Figure 3A). *LysM$^+$ Fbxw7$^{fl/fl}$* mice sacrificed on day 9 displayed significantly longer colons (Figure 3B), milder epithelial damage, and deceased areas of mucosal ulceration (Figure 3C and Supplemental Figure 2A) compared with *Fbxw7$^{fl/fl}$* littermates. Moreover, expression levels of the tight junction genes *Cldn1*, *Cldn2*, *Ocln*, and *Tjp1* (Supplemental Figure 2B) and of TJP1 protein (Supplemental Figure 2C) were significantly higher in the epithelia of *LysM$^+$ Fbxw7$^{fl/fl}$* mice compared with *Fbxw7$^{fl/fl}$* littermates after DSS treatment, which indicated that the epithelial barrier integrity was less disrupted in mice with myeloid-specific Fbxw7 deficiency. At the same time, *LysM$^+$ Fbxw7$^{fl/fl}$* mice showed significantly improved survival rates compared with *Fbxw7$^{fl/fl}$* littermates after 4% DSS treatment (Figure 3D), indicating that *Fbxw7* deficiency protects mice from DSS-induced colitis.

During the recovery period of intestinal inflammation, the rate of body weight gain was more rapid in *LysM$^+$ Fbxw7$^{fl/fl}$* mice than in *Fbxw7$^{fl/fl}$* littermates (Figure 3E). Moreover, *LysM$^+$ Fbxw7$^{fl/fl}$* mice had longer colon lengths than did their *Fbxw7$^{fl/fl}$* littermates (Figure 3F) on day 15. Similarly, TNBS-induced colon shortening, the disease activity index (DAI), body weight loss, and epithelial damage were also alleviated in *LysM$^+$ Fbxw7$^{fl/fl}$* mice compared with *Fbxw7$^{fl/fl}$* littermates (Supplemental Figure 3, A–D). These findings indicate that myeloid *Fbxw7* deficiency attenuates experimental colitis.

Fbxw7 deficiency decreases proinflammatory MPh accumulation. Microbiota-induced inflammation is critical for the regulation of intestinal homeostasis. To determine whether the decreased DSS colitis susceptibility in *LysM$^+$ Fbxw7$^{fl/fl}$* mice was mediated by shifts in gut microbiota, we analyzed the fecal microbiota composition in *LysM$^+$ Fbxw7$^{fl/fl}$* mice and *Fbxw7$^{fl/fl}$* littermates. The relative abundance of bacteria at the phylum level and the species composition cluster according to operational taxonomic units (OTUs) among *LysM$^+$ Fbxw7$^{fl/fl}$* mice and *Fbxw7$^{fl/fl}$* littermates are shown in Supplemental Figure 4A and Figure 4A, respectively. Moreover, microbial community diversity (Figure 4B) and microbial community composition (Supplemental Figure 4B) were not significantly different between *LysM$^+$ Fbxw7$^{fl/fl}$* mice and *Fbxw7$^{fl/fl}$* littermates. Furthermore, fecal microbiota were transferred from *LysM$^+$ Fbxw7$^{fl/fl}$* mice into *Fbxw7$^{fl/fl}$* mice by cohousing. At the end of the colitis induction period, cohoused *LysM$^+$ Fbxw7$^{fl/fl}$* mice still showed clear alleviation of DSS-induced colitis (Supplemental Figure 4, C–G) compared with cohoused *Fbxw7$^{fl/fl}$* or single-housed *Fbxw7$^{fl/fl}$* mice. These results demonstrated that decreased DSS-induced colitis susceptibility in *LysM$^+$ Fbxw7$^{fl/fl}$* mice was not due to the microbiome change.
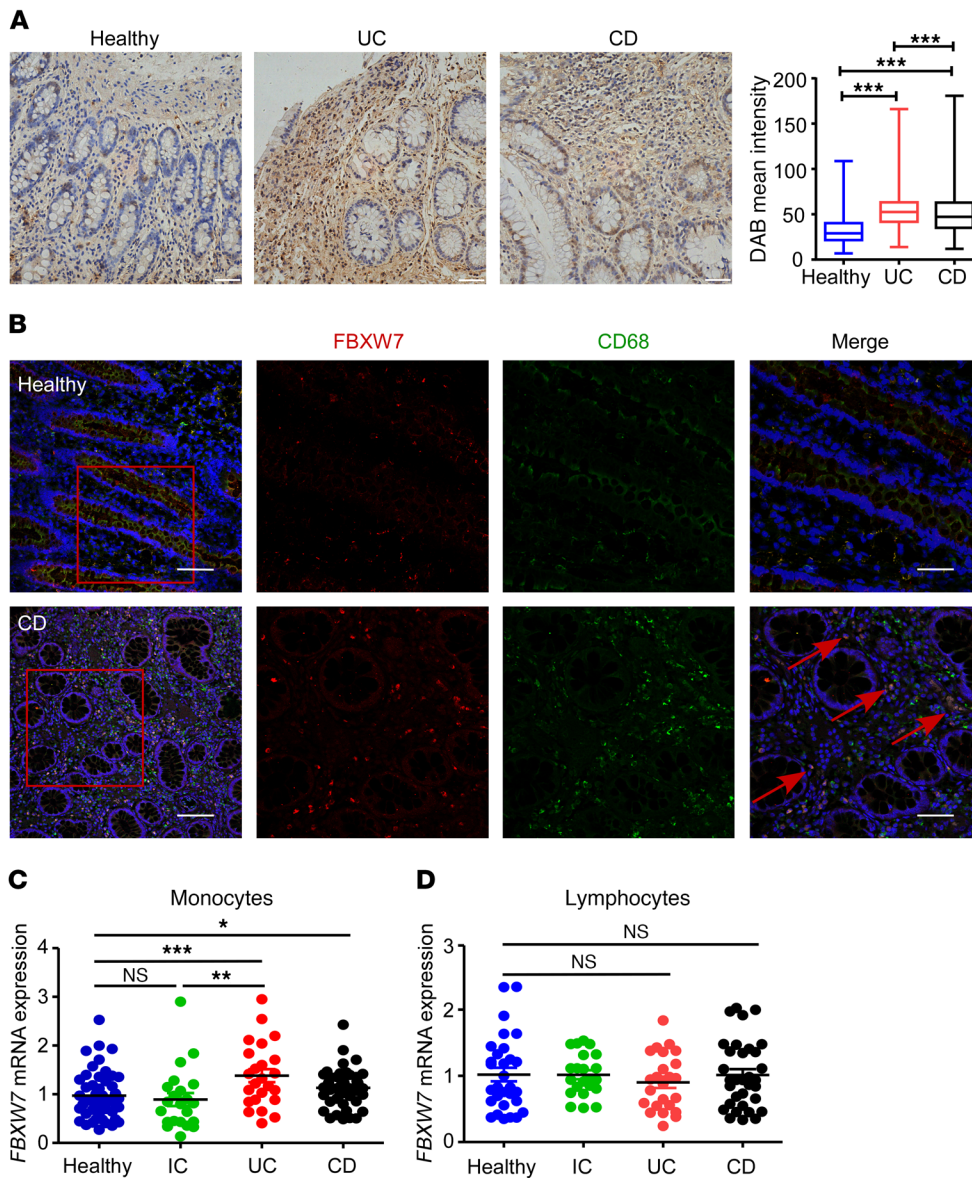
Figure 1. Increased FBXW7 expression in inflamed intestinal tissues in humans. (**A**) Representative immunohistochemical staining of paraffin-embedded sections of colon specimens obtained from colonic biopsies from patients with UC or CD and healthy controls. Comparison of staining intensity (TissueGnostics) among the groups is shown. Original magnification, ×40. Scale bar: 50 μm. (**B**) Immunofluorescence staining for FBXW7 (red), CD68 (green), and DAPI for nuclei (blue) in healthy human tissue and CD tissue. Scale bars: 100 μm (whole colon section) and 50 μm (enlarged insets). Red arrows point to CD68+ macrophages with high expression of FBXW7. *FBXW7* mRNA expression in peripheral blood monocytes (**C**) from healthy controls (n = 50) and from patients with IC (n = 22), UC (n = 24), or CD (n = 44), or in peripheral blood lymphocytes (**D**) from healthy controls (n = 30) and from patients with IC (n = 22), UC (n = 24), or CD (n = 33). *P < 0.05, **P < 0.01, and ***P < 0.001, by 1-way ANOVA with Tukey's multiple comparisons test. Data are presented as the mean ± SEM and are representative of 3 independent experiments.

We next investigated the changes in myeloid cell subpopulations in CLP during colitis development by analyzing CD11b+ CX3CR1hi resident macrophages and CD11b+CX3CR1int proinflammatory MPhs in the colon. We found that the accumulation of CX3CR1int proinflammatory MPhs (red) increased with the severity of intestinal inflammation and finally reached its highest proportion on day 9 after DSS treatment in WT mice (*Fbxw7fl/fl*) (Figure 4, C and D). Importantly, KO mice (*LysM+ Fbxw7fl/fl*) showed an obviously reduced accumulation of this CX3CR1int cell population compared with *Fbxw7fl/fl* littermates, starting the third day after DSS treatment, but we observed no difference in the frequency of CX3CR1hi resident macrophages (blue) in *LysM+Fbxw7fl/fl* and *Fbxw7fl/fl* littermates during the colitis period (Figure 4, C and D). In addition, the percentage and number of Ly6ChiCX3CR1int monocytes (Figure 4E) and the percentage of CD11b+Ly6G+ neutrophils in CLP (Supplemental Figure 5A) were lower in *LysM+Fbxw7fl/fl* mice than in *Fbxw7fl/fl* mice at the later, but not the early, stage of colitis, whereas the accumulation of CD103+

or CD103− DCs was similar in CLP of *LysM+ Fbxw7fl/fl* mice and their *Fbxw7fl/fl* littermates (Supplemental Figure 5B).

Given that neutrophils express high levels of Lyz2 and can be recruited to inflamed tissue to exert antimicrobial effects, the expression of FBXW7 was also increased in peripheral blood and CLP neutrophils from mice with colitis compared with healthy mice. We then examined whether the attenuated colitis in *LysM+ Fbxw7fl/fl* mice was related to the neutrophils. We found that depletion of neutrophils by anti-Ly6G Ab could not abrogate the reduced inflammation phenotype of *LysM+Fbxw7fl/fl* mice (Supplemental Figure 6, C–G). These findings indicated that the function of *Fbxw7* in colitis was not dependent on neutrophils.

To further confirm that the function of *Fbxw7* in colitis was dependent on macrophages, we depleted macrophages using clodronate-containing liposomes (CLs) (26, 27). Flow cytometric analysis confirmed a marked reduction in the percentages of local macrophages in mice treated with CLs (Supplemental Figure 7, A and B). The protective effect of myeloid
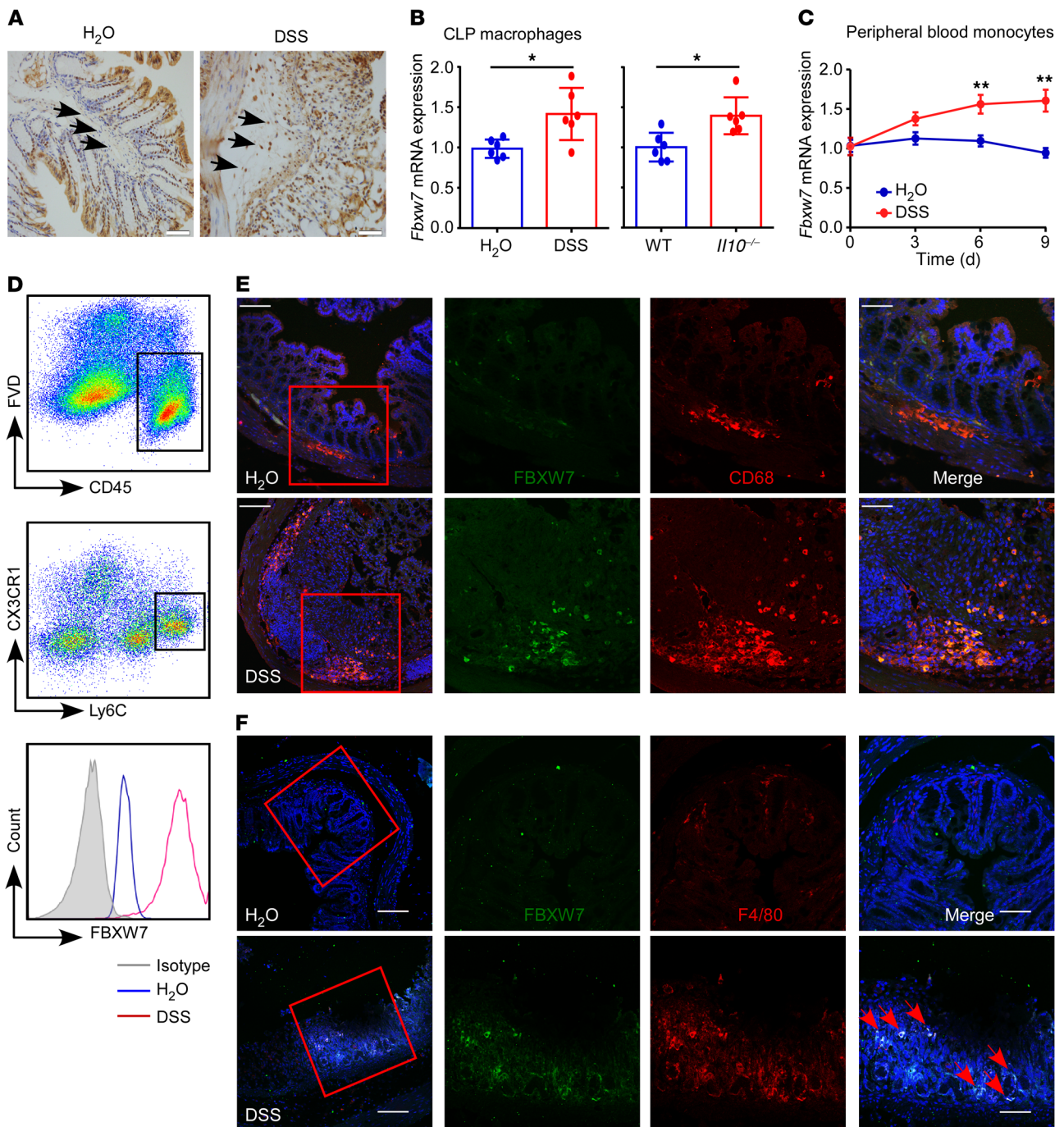
Figure 2. Increased FBXW7 expression in inflamed intestinal tissues in mice. (**A**) Representative immunohistochemical staining of colon specimens obtained from control mice and mice with colitis treated for 5 days with DSS. Scale bars: 50 μm. Arrows point to macrophages with high expression of FBXW7. (**B**) *Fbxw7* mRNA expression in CLP CD11b⁺CX3CR1⁺ macrophages from mice with DSS-induced colitis (day 9) and 12-week-old *Il10⁻/⁻* mice ($n = 6$). (**C**) Quantitative assessment of *Fbxw7* mRNA expression in peripheral blood monocytes from mice with colitis at different time points after DSS challenge ($n = 6$). (**D**) Representative flow cytometric analysis of FBXW7 expression in murine Ly6C^hi^CX3CR1^int^ colonic monocytes at steady and inflammatory states. FVD, Zombie Violet Fixable Viability Dye. Immunofluorescence staining for (**E**) FBXW7 (green), CD68 (red), and DAPI for nuclei (blue) and (**F**) FBXW7 (green), F4/80 (red), and DAPI for nuclei (blue) in colon tissues from control mice and mice with DSS-induced colitis. Scale bars: 100 μm (whole colon sections) and 50 μm (enlarged insets). Red arrows point to F4/80⁺ macrophages with high expression of FBXW7. *$P < 0.05$ and **$P < 0.01$, by unpaired, 2-tailed Student's *t* test. Data are presented as the mean ± SD of at least 3 independent experiments.

Fbxw7 deficiency in colitis disappeared in the absence of macrophages compared with that seen in the control cohort (Figure 4, F–I), which was further confirmed by analysis of tight junction protein expression (Supplemental Figure 7C) as well

as the production of inflammatory cytokines during colonic inflammation (Supplemental Figure 7D). We also confirmed the increased expression of *Fbxw7* in sorted CX3CR1^hi^ resident macrophages and CX3CR1^int^ MPhs from C57BL/6 mice with
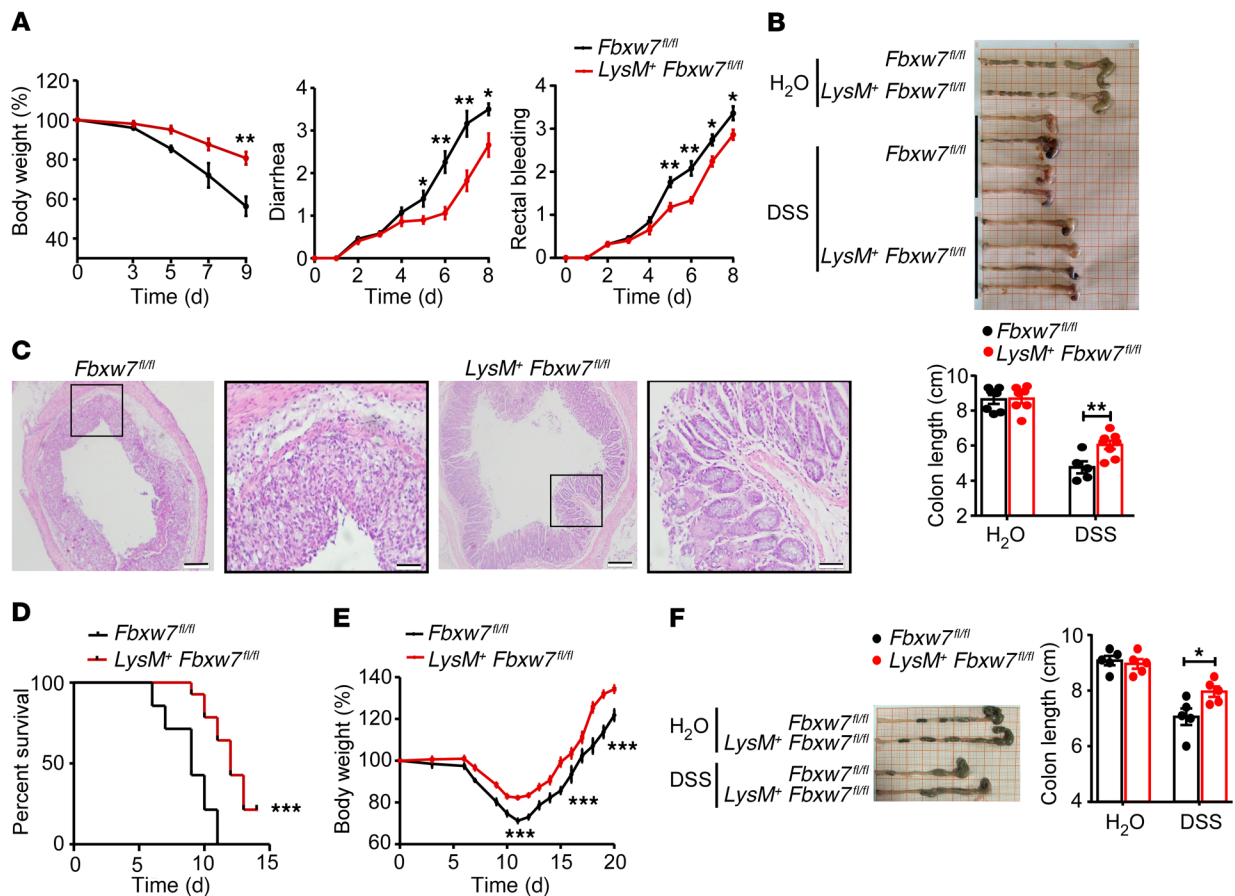
Figure 3. LysM⁺ Fbxw7^{fl/fl} mice show attenuated experimental colitis. *Fbxw7^{fl/fl}* and *LysM⁺ Fbxw7^{fl/fl}* mice were administered water or 3% DSS for 7 days to induce acute colitis, followed by a 2-day recovery period on normal drinking water. (**A**) Body weight changes, diarrhea, and rectal bleeding scores were assessed daily as described in Methods (*n* = 5). (**B**) Gross morphology of colons from *Fbxw7^{fl/fl}* and *LysM⁺ Fbxw7^{fl/fl}* mice. Colon lengths were measured on day 9 (*n* ≥ 5). (**C**) H&E-stained images of colon sections. Scale bars: 200 μm (whole colon section) and 50 μm (enlarged insets). (**D**) *Fbxw7^{fl/fl}* and *LysM⁺ Fbxw7^{fl/fl}* mice were administered 4% DSS to induce acute colitis. Survival of mice was monitored until day 15 (*n* = 10). ***P < 0.001, by log-rank test. (**E**) Body weight changes during intestinal inflammation and the recovery period (*n* = 5). (**F**) Length of colons from *Fbxw7^{fl/fl}* and *LysM⁺ Fbxw7^{fl/fl}* mice sacrificed after 7 days of 3% DSS treatment and 8 days' recovery with drinking water (*n* = 5). Data are presented as the mean ± SEM and are representative of 3 independent experiments. *P < 0.05, **P < 0.01, and ***P < 0.001, by unpaired, 2-tailed Student's *t* test (**A**, **B**, **E**, and **F**).

DSS-induced colitis compared with expression levels in healthy control mice (Supplemental Figure 7E).

Taken together, these results suggested that myeloid *Fbxw7* deficiency leads to a marked reduction in the accumulation of proinflammatory MPhs in the colitis microenvironment.

Fbxw7 *deficiency downregulates Ccl2 and Ccl7 in resident macrophages.* The abnormal phagocytosis of invading microbes by resident macrophages could induce excessive inflammation (28). We first confirmed that *Fbxw7* deficiency did not affect the phagocytic function of macrophages by detecting the phagocytotic efficiency of bone marrow–derived macrophages (BMDMs) from *LysM⁺ Fbxw7^{fl/fl}* mice and *Fbxw7^{fl/fl}* littermates (Supplemental Figure 8A) and did not influence the expression of phagocytosis-related genes (*Mfge8, Timd4, Anxa1*) in primary peritoneal and CLP macrophages (Supplemental Figure 8B). We found that *Fbxw7* deficiency in macrophages also did not affect the survival of macrophages after serum depletion (Supplemental Figure 8C).

The inflammatory cytokines TNF-α and IL-6 are predominantly produced by inflammatory MPhs during colitis (3). We

therefore examined whether *Fbxw7* deficiency decreases the expression of cytokines. An ELISA revealed comparable inflammatory cytokine production levels (TNF-α, IL-6, IL-10) in *LysM⁺ Fbxw7^{fl/fl}* and *Fbxw7^{fl/fl}* colon tissue 5 days after DSS challenge (Figure 5A and Supplemental Figure 9A), and analysis of mRNA expression of cytokine genes in BMDMs from *LysM⁺ Fbxw7^{fl/fl}* and *Fbxw7^{fl/fl}* mice revealed no significant differences (Supplemental Figure 9B). Local inflammation and tissue damage in UC and CD are affected by local expression of specific chemokines within IBD tissues (29), and DSS-induced colitis correlates directly with the CCR2-mediated accumulation of MPhs (30). To address the mechanisms involved in the downregulation of intestinal inflammation by myeloid deficiency of *Fbxw7*, we sorted CX3CR1^hi resident macrophages, CX3CR1^int proinflammatory MPhs, and Ly6C^hi monocyte populations. We found that CX3CR1^hi resident macrophages expressed markedly higher amounts of chemokines than did those in CX3CR1^int proinflammatory MPhs (Supplemental Figure 9C). Then, transcriptomic analysis of macrophages from *LysM⁺ Fbxw7^{fl/fl}* mice and *Fbxw7^{fl/fl}* littermates identified differentially
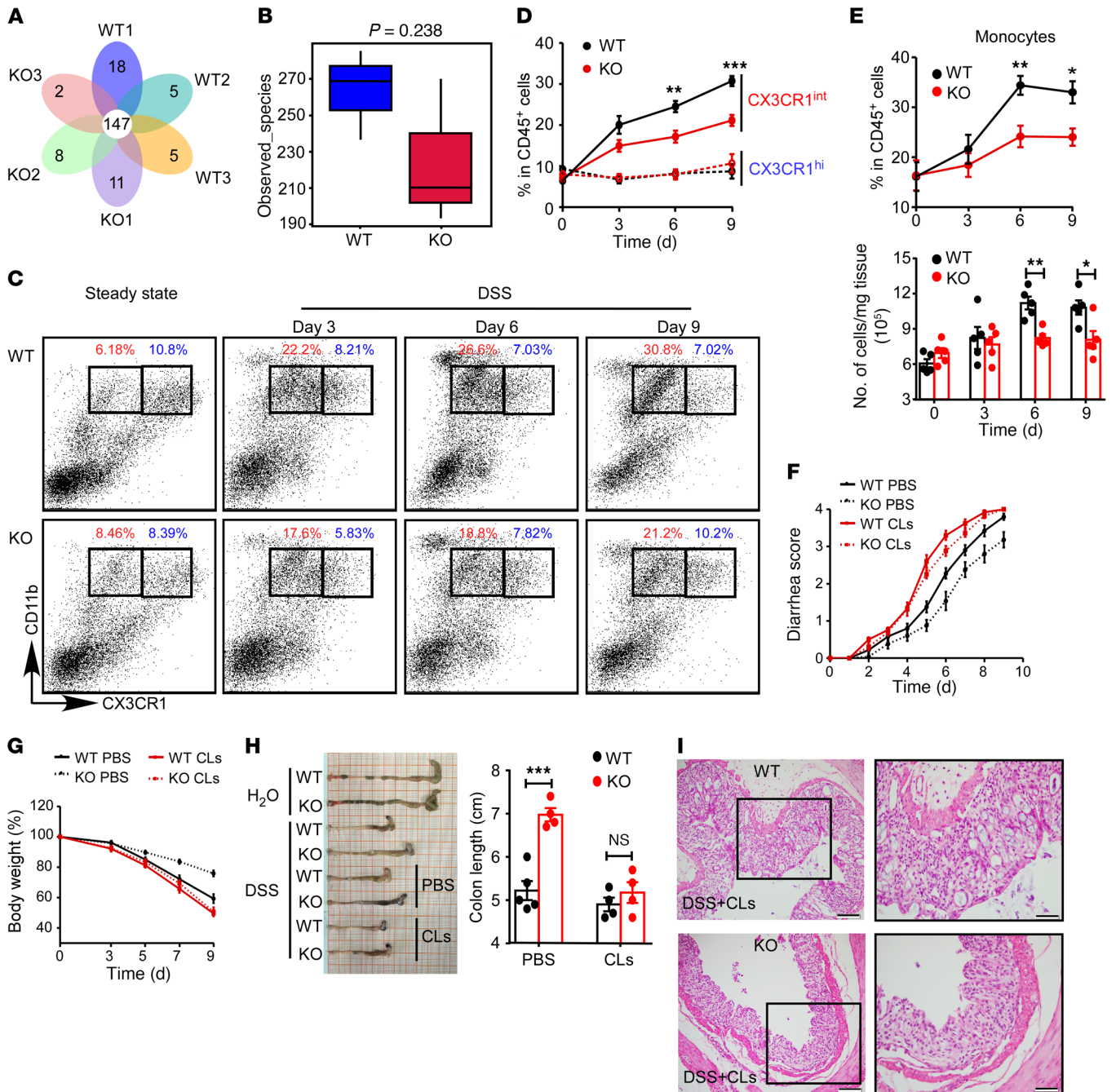
Figure 4. *Fbxw7* deficiency decreases the accumulation of CX3CR1^int proinflammatory MPhs. (**A**) Venn diagram of *Fbxw7^fl/fl* (WT) and *LysM⁺ Fbxw7^fl/fl* (KO) groups showing unique and shared OTUs for bacterial sequences based on normalized sequences and 97% sequence similarity (*n* = 3). (**B**) Analysis of α diversity (observed_species) in WT and KO groups (*n* = 3). The *P* value was calculated from analysis of an independent samples Student's *t* test. (**C**) Representative flow cytometric plots gated on CD45⁺ living cells isolated from CLP from WT and KO mice on days 0, 3, 6, and 9 after DSS challenge. CD11b⁺CX3CR1^hi resident macrophages (blue); CD11b⁺CX3CR1^int MPhs (red). (**D**) Dynamics of CD11b⁺CX3CR1^hi macrophages and CD11b⁺CX3CR1^int MPh infiltration into CLP after DSS treatment (*n* = 5 for any time point). (**E**) Percentage and number of Ly6C^hiCX3CR1^int monocytes in inflamed colon after DSS treatment (*n* = 5 for any time point). Then, macrophages were depleted by CLs in WT and KO mice that were subjected to 3% DSS treatment for 7 days, and the mice were sacrificed on day 9. Diarrhea score (**F**) and body weight changes (**G**) were assessed daily (*n* = 5). (**H**) Gross morphology of colons from mice on day 9 after DSS treatment and colon length measurements (*n* = 5). (**I**) H&E-stained images of colon sections from mice with colitis. Scale bars: 200 μm (whole colon sections) and 50 μm (enlarged insets). (**C–H**) Data are expressed as the mean ± SEM and are representative of at least 3 independent experiments. **P* < 0.05, ***P* < 0.01, and ****P* < 0.001, by unpaired, 2-tailed Student's *t* test .

expressed genes and also revealed that myeloid *Fbxw7* deficiency led to markedly decreased expression of various inflammation-related genes, among which *Ccl2* and *Ccl7* are the most important (Figure 5B). The decrease in cytokine expression detected in colon tissue from *LysM*[+] *Fbxw7*^{fl/fl} mice at the later phase of colitis (9 days after DSS treatment) (Figure 5A) might be the consequence of the substantial decrease in inflammatory MPh infiltration. Compared with *Fbxw7*^{fl/fl} littermates, *LysM*[+] *Fbxw7*^{fl/fl} mice had markedly lower expression levels of *Ccl2* and *Ccl7* in the resident macrophage population, whose functions were mainly involved in the recruitment of monocytes (Figure 5C). Quantitative reverse transcription PCR (qRT-PCR) (Supplemental Figure 9, D and E) and ELISA (Figure 5D and Supplemental Figure 9F) further confirmed that myeloid deficiency of *Fbxw7* resulted in lower levels of CCL2 and CCL7 in macrophages from mice with colitis. Moreover, macrophage-depleted *LysM*[+] *Fbxw7*^{fl/fl} mice and *Fbxw7*^{fl/fl} littermates showed similar expression levels of the chemokines CCL2 and CCL7 (Figure 5D). We also observed a significant correlation between *Fbxw7* mRNA and *Ccl2* mRNA levels in colonic mucosal samples from patients with UC in the GEO database (Supplemental Figure 9G). Collectively, these results suggested that myeloid *Fbxw7* deficiency decreases the production of *Ccl2* and *Ccl7* in resident macrophages.

Monocyte migration from peripheral blood during infection or inflammation requires CCL2/CCL7/CCR2 signaling (31); therefore, we performed a Transwell migration assay to compare the chemoattractive function of resident macrophages from *LysM*[+] *Fbxw7*^{fl/fl} mice and *Fbxw7*^{fl/fl} littermates in vitro (Supplemental Figure 10, A and B) and found that *LysM*[+] *Fbxw7*^{fl/fl} resident macrophages recruited fewer monocytes than did macrophages from *Fbxw7*^{fl/fl} littermates in a Transwell assay (Figure 5E and Supplemental Figure 10C). Furthermore, CCL2 and CCL7 production was decreased in the culture supernatant of CX3CR1[hi] resident macrophages from *LysM*[+] *Fbxw7*^{fl/fl} mice compared with macrophages from *Fbxw7*^{fl/fl} littermates (Figure 5F). Compared with resident macrophages, the culture supernatant of proinflammatory MPhs from both *LysM*[+] *Fbxw7*^{fl/fl} and *Fbxw7*^{fl/fl} littermate mice showed a weaker ability of the macrophages to recruit monocytes (Figure 5E and Supplemental Figure 10C) with lower levels of chemokines (Figure 5F). Importantly, neutralization of CCL2 and CCL7 abrogated the difference in the monocyte-recruiting ability of *Fbxw7*^{fl/fl} and *LysM*[+] *Fbxw7*^{fl/fl} resident macrophages (Figure 5G and Supplemental Figure 10D). This observation suggested that decreased production of CCL2 and CCL7 in *LysM*[+] *Fbxw7*^{fl/fl} resident macrophages contributed to the reduced recruitment of Ly6C^{hi} monocytes. Furthermore, anti-CCL2 and anti-CCL7 Abs decreased the number of inflammatory MPhs that infiltrated into the colons of both *Fbxw7*^{fl/fl} and *LysM*[+] *Fbxw7*^{fl/fl} mice (Supplemental Figure 11, A and B) and abrogated the alleviated colitis phenotype of *LysM*[+] *Fbxw7*^{fl/fl} mice (Figure 5, H and I, and Supplemental Figure 11, C and D). Moreover, we adoptively transferred mixed *Fbxw7*^{fl/fl} and *LysM*[+] *Fbxw7*^{fl/fl} monocytes into *Fbxw7*^{fl/fl} and *LysM*[+] *Fbxw7*^{fl/fl} recipient mice (Supplemental Figure 11E). Flow cytometric analysis revealed a failure of monocyte recruitment in the inflamed colons of *LysM*[+] *Fbxw7*^{fl/fl} recipient mice when compared with their *Fbxw7*^{fl/fl} littermates (Figure 5J). Collectively, these data further support the idea that *Fbxw7* deficiency decreases the expression of CCL2 and CCL7 in resident macrophages and

thereby reduces the accumulation of proinflammatory MPhs during colitis progression.

FBXW7 interacts with EZH2. To identify the mechanisms regulating CCL2 and CCL7 production in colon-resident macrophages, we assessed the activation of NF-κB and HIF-1α (32, 33) signaling pathways in BMDMS during the LPS-induced response. We found no potent difference in these signaling pathways between *Fbxw7*^{fl/fl} and *LysM*[+] *Fbxw7*^{fl/fl} BMDMs after LPS stimulation (Figure 6, A and B). These results raise the possibility of epigenetic regulation of the *Ccl2* and *Ccl7* genes in response to inflammatory stimuli. We next assessed changes in histone modifications and found that the modification of H3K27me3 was markedly increased in *LysM*[+] *Fbxw7*^{fl/fl} BMDMs compared with *Fbxw7*^{fl/fl} BMDMs after LPS stimulation (Figure 6C). EZH2 was found to be an important enzyme for H3K27me3 (34), and we observed a decrease in the expression of EZH2 protein in BMDMs after LPS challenge (Supplemental Figure 12A). The expression of EZH2 was also decreased in CD11b^{+} macrophages from CLP of mice with IBD compared with macrophages from healthy controls (Supplemental Figure 12B). We speculated that EZH2 protein expression negatively correlates with FBXW7 levels in CLP macrophages. We found higher EZH2 protein expression levels in *Fbxw7*-deficient BMDMs than in *Fbxw7*^{fl/fl} BMDMs upon LPS stimulation (Figure 6D). Furthermore, the interaction of endogenous EZH2 and FBXW7 in BMDMs was increased after LPS challenge (Figure 6E). We consistently found that FBXW7 colocalized with EZH2 upon LPS stimulation in BMDMs (Figure 6F).

FBXW7 recognizes and binds to substrates through a stretch of eight WD40 repeat domains (34), and the binding consensus motif (T/S)PXX(S/T/D/E) has been identified in several FBXW7 substrates, including c-Myc, cyclin E1, and c-Jun (36–38). Protein motif analysis showed that 2 domains in the EZH2 protein sequence might be the FBXW7 binding motif (Figure 6G). To determine whether those amino acid sequences were required for FBXW7 recognition and ubiquitination, we constructed 3 mutants of EZH2, in which serine residues at positions 261, 265, and/or 367, and 371 were replaced with glycine residues. The results showed that mutant EZH2 (261, 265A) and mutant EZH2 (367, 371A) bound to FBXW7 less efficiently than did EZH2, and that mutant EZH2 (261, 265, 367, and 371) could not bind to FBXW7 (Figure 6H). These results strongly suggest that the serine at positions 261, 265, 367, and 371 of EZH2 was critical for its interaction with FBXW7.

FBXW7 mediates the degradation and ubiquitination of EZH2. We confirmed that EZH2 was the target of FBXW7 in macrophages, as there was no significant difference between *Fbxw7*^{fl/fl} and *LysM*[+] *Fbxw7*^{fl/fl} BMDMs in terms of *Ezh2* mRNA expression levels upon LPS stimulation (Supplemental Figure 12C). However, we found that the decrease in EZH2 protein expression after LPS stimulation (Supplemental Figure 12A) was completely blocked by the proteasome inhibitor MG132 (Figure 7A). A cycloheximide chase assay showed that FBXW7 deficiency extended the half-life of endogenous EZH2 protein in BMDMs (Figure 7, B and C). These data indicated that FBXW7 might induce EZH2 degradation through proteasomes. Exogenously expressed EZH2 was degraded by overexpressed FBXW7 in HEK293 cells, which was also abrogated by MG132 (Figure 7D).
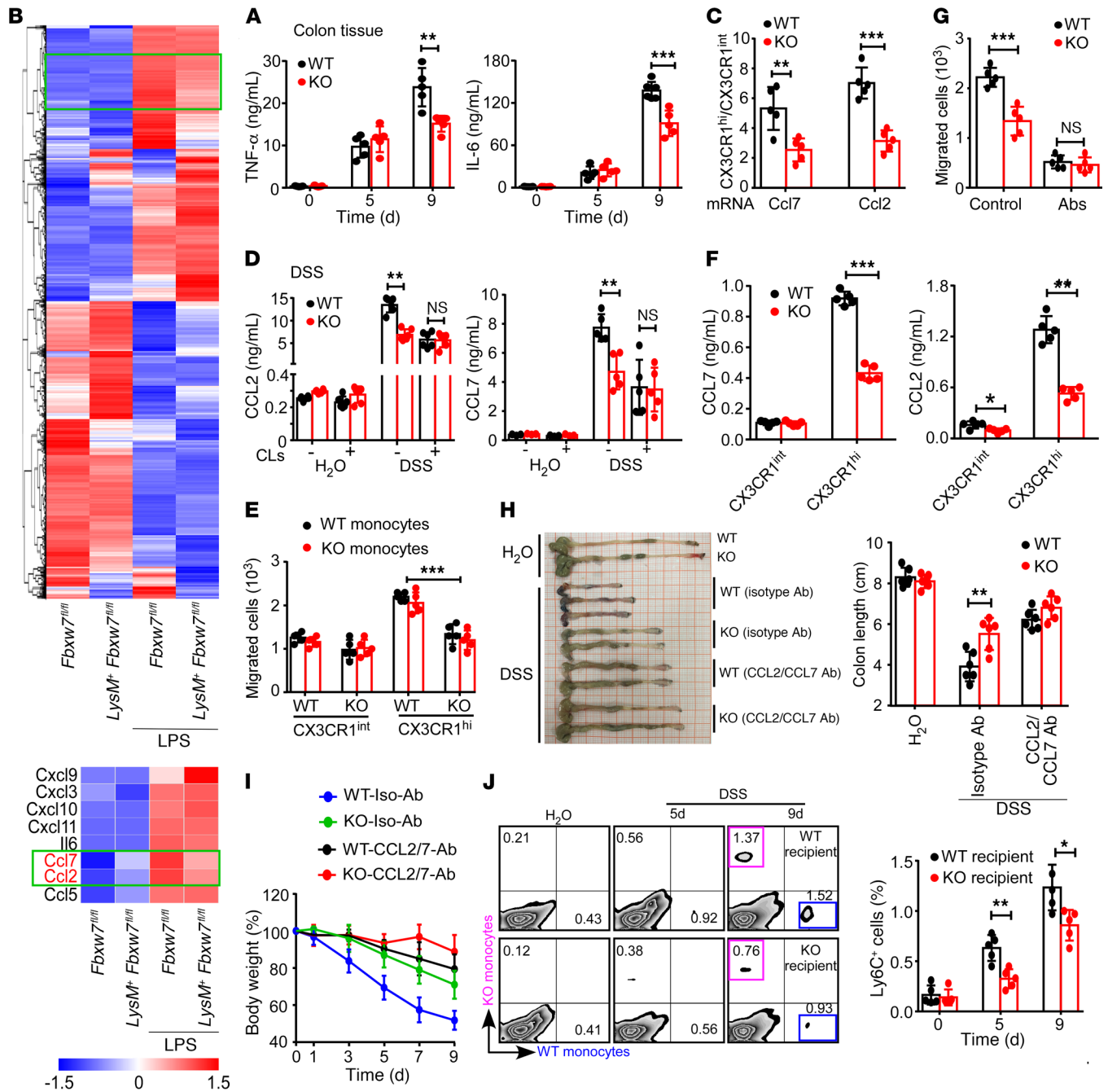
Figure 5. *Fbxw7* deficiency downregulates CCL2 and CCL7 in resident macrophages. (**A**) Colon tissue was cultured overnight, and cytokines in the super-natant were measured by ELISA (*n* = 5). (**B**) Heatmap showing expression changes of inflammation-related genes in BMDMs from *LysM⁺ Fbxw7ᶠˡ/ᶠˡ* mice and *Fbxw7ᶠˡ/ᶠˡ* littermates. The expression profile is accompanied by a colored bar indicating the standardized log₂ intensities. BMDMs were isolated from *LysM⁺ Fbxw7ᶠˡ/ᶠˡ* mice and *Fbxw7ᶠˡ/ᶠˡ* littermates and stimulated with LPS (100 ng/mL) for the transcriptomic assay. (**C**) CD11b⁺CX3CR1ʰⁱ resident macrophages and CD11b⁺CX3CR1ⁱⁿᵗ proinflammatory MPHs were sorted from CLP of *Fbxw7ᶠˡ/ᶠˡ* (WT) and *LysM⁺ Fbxw7ᶠˡ/ᶠˡ* (KO) mice (*n* = 5) after 5 days of DSS or H₂O adminis-tration, and gene expression levels were quantified by gene-specific amplification and qRT-PCR. The ratio of *Ccl2* and *Ccl7* expression in CX3CR1ʰⁱ resident macrophages to *Ccl2* and *Ccl7* expression in CX3CR1ⁱⁿᵗ MPHs is shown. (**D**) Colonic tissues of WT and KO mice treated with DSS were cultured overnight, CCL2 and CCL7 expression in the supernatant was measured by ELISA (*n* = 5). (**E**) In a Transwell assay, the number of monocytes in the lower chamber recruited by supernatant of CLP-derived CX3CR1ʰⁱ resident macrophages and CX3CR1ⁱⁿᵗ proinflammatory MPHs was counted by flow cytometry (*n* = 5). (**F**) Concentration of CCL2 and CCL7 in the culture medium of CX3CR1ʰⁱ macrophages and CX3CR1ⁱⁿᵗ MPHs (*n* = 5). (**G**) Number of monocytes in the lower chamber recruited by the supernatant of CX3CR1ʰⁱ resident macrophages from WT mice, with or without anti-CCL2 and anti-CCL7 Ab treatment (*n* = 5). (**H**) Gross morphology of colons from *Fbxw7ᶠˡ/ᶠˡ* and *LysM⁺ Fbxw7ᶠˡ/ᶠˡ* mice, with or without anti-CCL2 and anti-CCL7 Ab treatment and colon length measurements on day 9 (*n* = 5). (**I**) Body weight changes were assessed daily (*n* = 5). (**J**) The percentages of labeled WT and KO monocytes gated on CD45⁺Ly6Cʰⁱ living cells from DSS-challenged recipient mice (*n* = 5) were analyzed by flow cytometry. Graph shows a summary of the percentages of labeled WT monocytes recruited to the CLP of WT and KO recipient mice on day 5 or 9 after DSS treatment. Data are presented as the mean ± SD and are representative of 3 independent experi-ments. *P < 0.05, **P < 0.01, and ***P < 0.001, by unpaired, 2-tailed Student's *t* test.
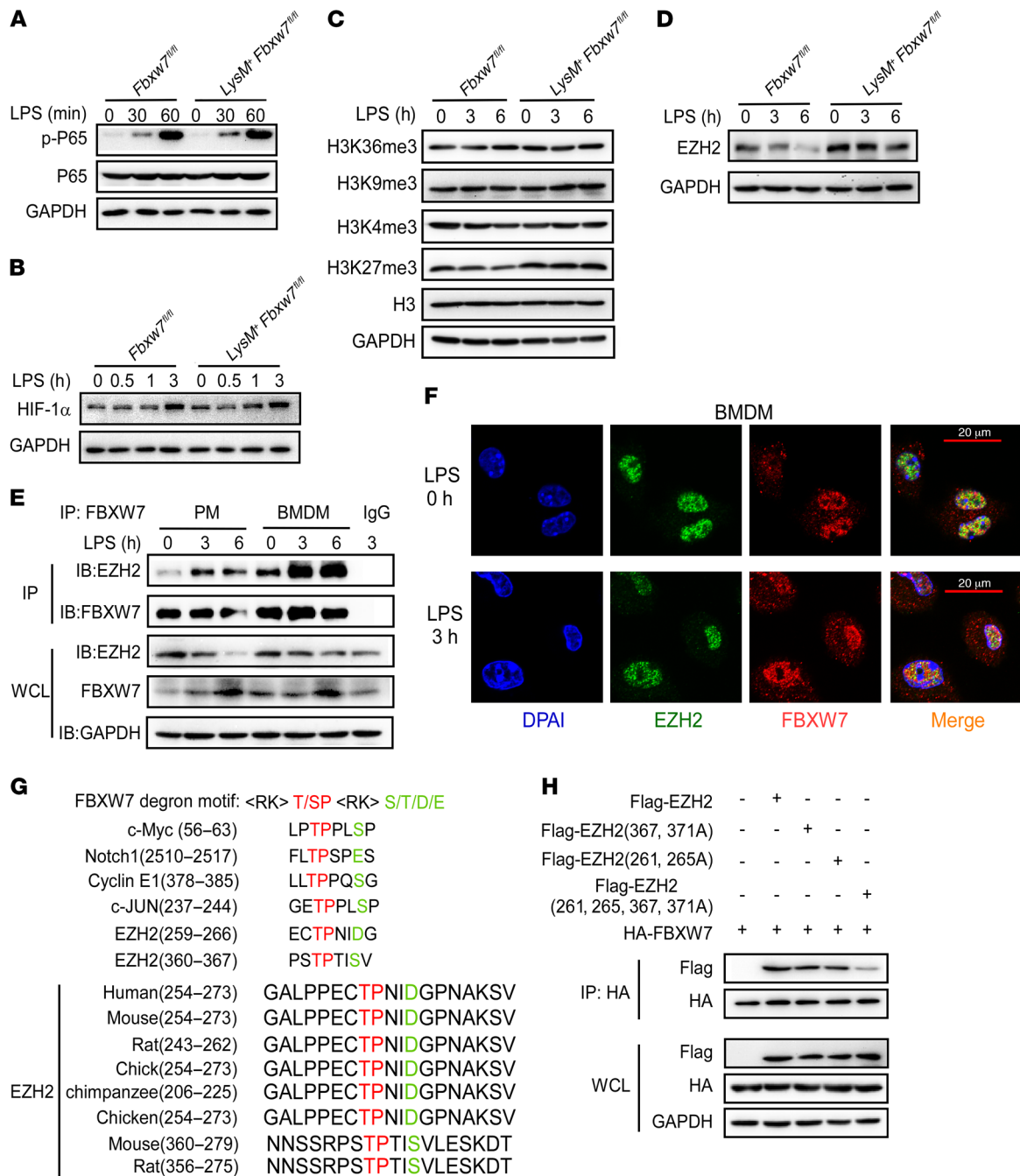
Figure 6. FBXW7 interacts with EZH2. Immunoblot analysis of phosphorylated P65 (p-P65) and total P65 (**A**), HIF-1α (**B**), H3 histone modification (**C**), and histone methyltransferase EZH2 protein levels (**D**) in lysates of BMDMs from *Fbxw7*^{fl/fl} and *LysM*+ *Fbxw7*^{fl/fl} mice stimulated with LPS for the indicated durations. (**E**) Coimmunoprecipitation (IP) and immunoblot (IB) of BMDMs stimulated with LPS for the indicated durations. (**F**) Confocal microscopic imaging of BMDMs that were stimulated with LPS and labeled with Abs against the appropriate protein. (**G**) Sequence alignment of EZH2 with FBXW7 degron motif (<RK>S/TP<RK>XS/T/E/D), where X and <RK> are any amino acid, except arginine (R) or lysine (K). (**H**) Coimmunoprecipitation and immunoblot analysis of HEK293T cells transfected with HA-FBXW7 along with a vector for Flag-EZH2 (WT), Flag-EZH2 (261 and 265A), Flag-EZH2 (367 and 371A), and Flag-EZH2 (261 and 265, 367, and 371A, 4A). and treated with MG132, followed by immunoprecipitation with anti–HA-M2 beads. All data are representative of at least 3 independent experiments.

However, FBXW7 could not decrease the expression of mutant EZH2 (position 4A) (Figure 7E). Collectively, these results indicated that EZH2 could be degraded by FBXW7 via the ubiquitin-proteasome system. Our study to determine whether FBXW7 functions as an E3 ubiquitin ligase of EZH2 revealed that the

ubiquitination of EZH2 was mediated by FBXW7 in a dose-dependent manner (Figure 7F). FBXW7 could induce K48-linked polyubiquitination of EZH2 (Figure 7G). Furthermore, FBXW7 deficiency in macrophages almost canceled K48-linked polyubiquitination of endogenous EZH2 compared with WT
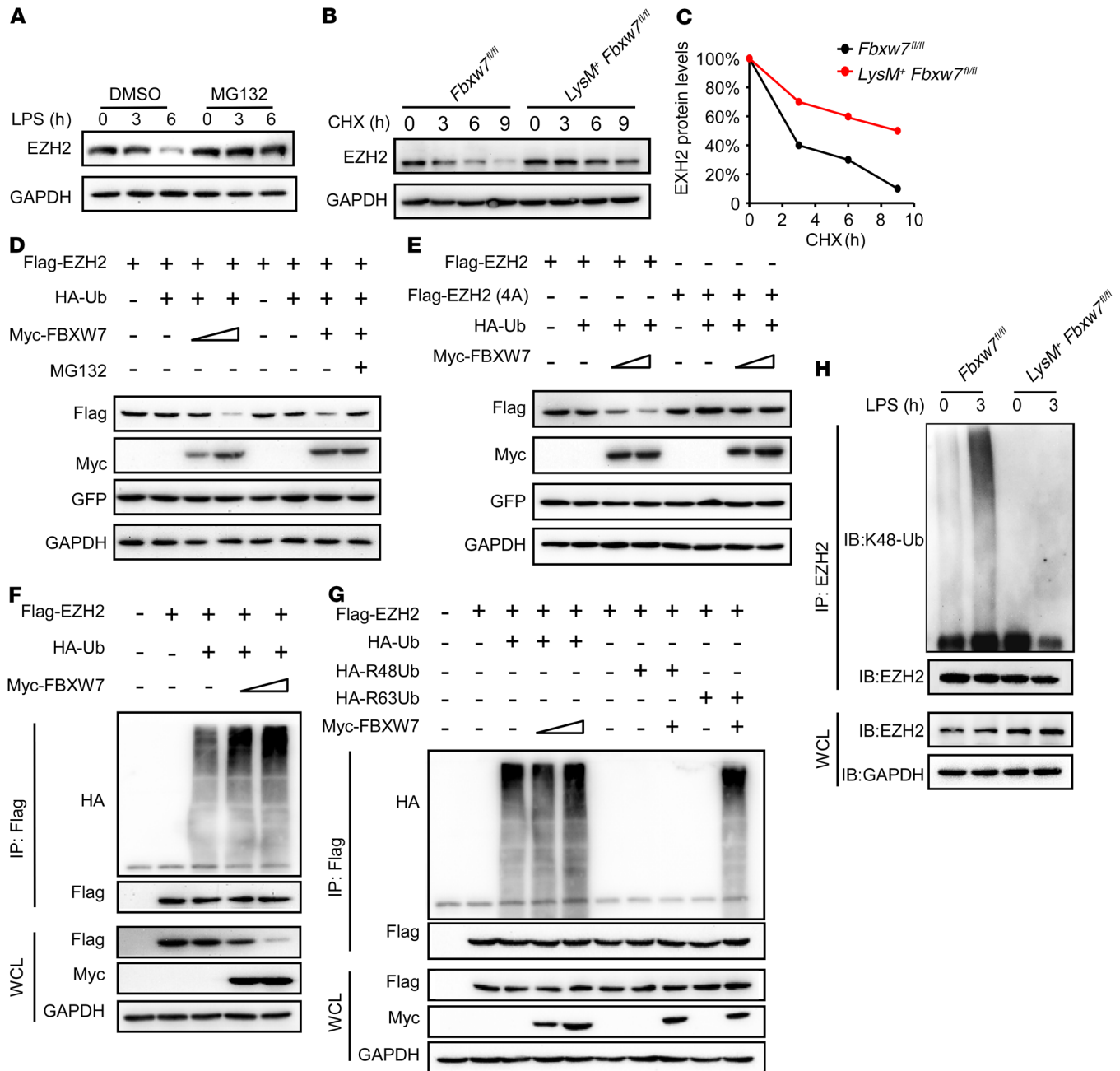
Figure 7. FBXW7 mediates the ubiquitination of EZH2 in macrophages. (**A**) Immunoblot analysis of EZH2 expression in BMDMs treated or not with MG132 for 8 hours and stimulated with LPS for the indicated durations. (**B**) Immunoblot analysis of EZH2 in lysates of *Fbxw7*^{fl/fl} and *LysM+ Fbxw7*^{fl/fl} BMDMs treated with CHX (40 μg/mL) for the indicated durations after stimulation with LPS for 1 hour. (**C**) Quantification of relative EZH2 protein levels. (**D**) Immunoblot analysis of HEK293T cells cotransfected for 36 hours with Myc-FBXW7 plus Flag-EZH2, HA-Ub, and GFP vectors treated or not with MG132. (**E**) Immunoblot analysis of HEK293T cells cotransfected for 36 hours with Myc-FBXW7, HA-Ub, and GFP, along with a vector for Flag-EZH2 and Flag-EZHh2 (261, 265, 367, and 371A, 4A). (**F**) Immunoblot analysis of the ubiquitination of EZH2 in HEK293T cells cotransfected with Flag-EZH2, HA-Ub, and increasing concentrations (wedge) of vectors for the Myc-FBXW7 constructs, and treated with MG132 for 6 hours before cell harvesting. (**G**) Immunoblot analysis of the ubiquitination of EZH2 in HEK293T cells cotransfected with Flag-EZH2, Myc-FBXW7, HA-Ub, the mutant ubiquitin HA-R48 Ub, or HA-R63 Ub, and treated with MG132 before cell harvesting. (**H**) Immunoblot analysis of the K48 ubiquitination of EZH2 in *Fbxw7*^{fl/fl} and *LysM+ Fbxw7*^{fl/fl} BMDMs stimulated with LPS. Data are representative of at least 3 independent experiments.

macrophages (Figure 7H). Together, these data demonstrate that FBXW7 promotes K48-linked polyubiquitination and proteasome degradation of EZH2 in macrophages.

EZH2 inhibits macrophage Ccl2 and Ccl7 expression by H3K27me3 modification. EZH2 has been shown to be recruited to the proxi-

mal promoter of the *Ccl2* gene in a clock gene BMAL1–dependent manner (39). We hypothesized that FBXW7 increases the expression of CCL2 and CCL7 chemokines by decreasing the protein levels of EZH2. *Ezh2* was knocked down by Ezh2 siRNA (siEzh2) in BMDMs, siEzh2 reduced expression of EZH2 and H3K27me3
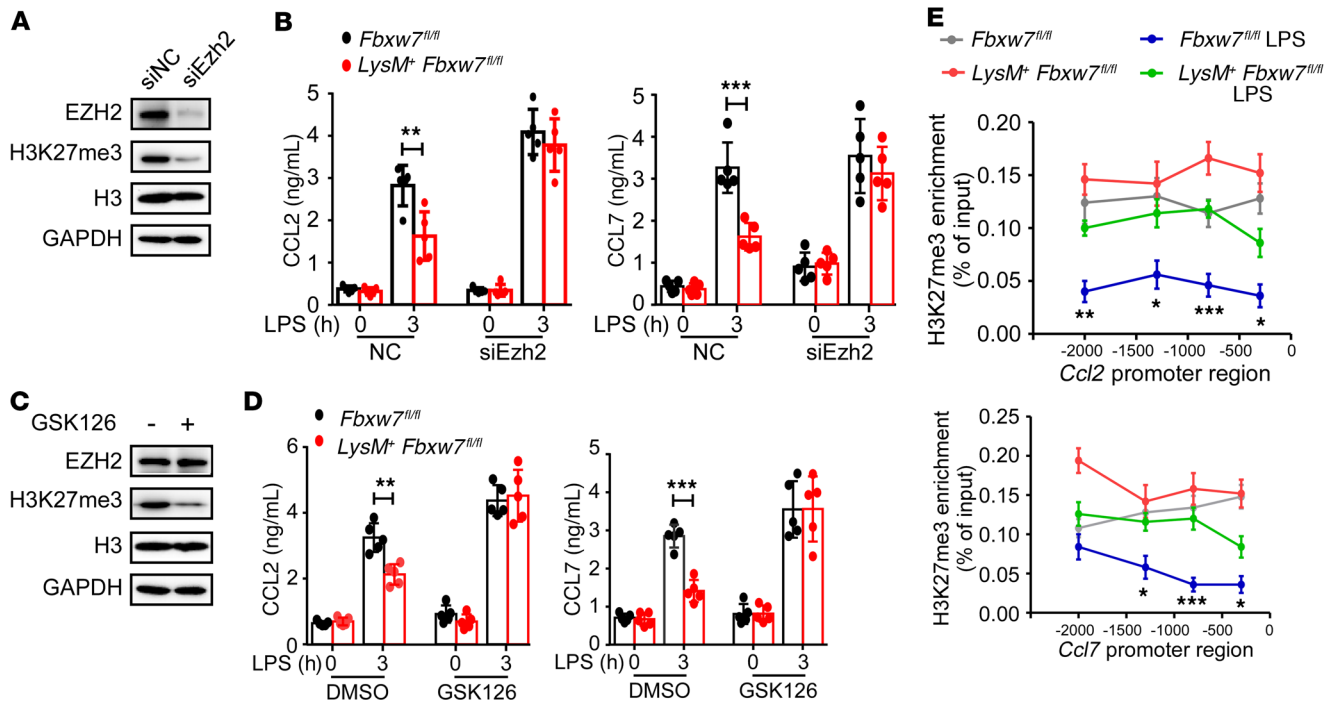
Figure 8. EZH2 inhibits macrophage *Ccl2* and *Ccl7* expression through H3K27me3 modification. (**A**) *Ezh2* in BMDMs was silenced with control siRNA (siNC) or *Ezh2*-specific siRNA (siEzh2) for 48 hours. The effects of siEzh2 on *Ezh2* expression and H3K27me3 modification in BMDMs were analyzed by immunoblot. (**B**) The concentration of CCL2 and CCL7 in the culture medium of *Fbxw7^fl/fl* and *LysM^+ Fbxw7^fl/fl* BMDMs after siEzh2 and LPS treatment was quantified by ELISA (*n* = 5). (**C**) GSK126 or DMSO (10 μM) was added to the cell culture medium for 2 days, and EZH2, H3K27me3, and H3 levels were detected by immunoblot assay. (**D**) The concentration of CCL2 and CCL7 in the culture medium of *Fbxw7^fl/fl* and *LysM^+ Fbxw7^fl/fl* BMDMs after GSK126 and LPS treatment was quantified by ELISA (*n* = 5). (**E**) ChIP assay for enrichment of H3K27me3 on the promoters of *Ccl2* and *Ccl7* in BMDMs, followed by LPS treatment. Data are presented as the mean ± SD and are representative of at least 3 independent experiments. *$P < 0.05$, **$P < 0.01$, and ***$P < 0.001$, by unpaired, 2-tailed Student's *t* test.

levels as compared with the control siRNA (siNC) (Figure 8A). Knockdown of *Ezh2* enhanced *Ccl2* and *Ccl7* mRNA expression in BMDMs and mitigated the difference in LPS-induced CCL2 and CCL7 expression between *Fbxw7^fl/fl* and *LysM^+ Fbxw7^fl/fl* BMDMs (Figure 8B). To test the direct effect of EZH2-associated H3K27me3 on expression of CCL2 and CCL7, we treated BMDMs with GSK126, an EZH2-specific competitive inhibitor compound (40), which induced loss of EZH2-associated H3K27me3, without any change in EZH2 protein abundance (Figure 8C). Treatment with GSK126 also showed consistently similar results with siEzh2 (Figure 8D). These data indicate that FBXW7 regulates CCL2 and CCL7 expression via EZH2-associated H3K27me3. A ChIP assay revealed greater H3K27me3 modification in the proximal promoter areas of *Ccl2* and *Ccl7* in *LysM^+ Fbxw7^fl/fl* BMDMs than in those in *Fbxw7^fl/fl* BMDMs (Figure 8E). These data suggest that FBXW7 promotes CCL2 and CCL7 chemokine expression by inhibiting EZH2-dependent methylation of H3K27 at the *Ccl2* and *Ccl7* gene promoters.

Reducing Fbxw7 expression alleviates colitis. The results described above demonstrated that FBXW7 expression was positively correlated with the severity of colitis, underscoring the therapeutic potential of FBXW7. To further explore the therapeutic importance of FBXW7 in colitis, recombinant adeno-associated virus (AAV-shFbxw7 or AAV-shNC vector as a control) was injected into the proximal bowel in mice. High-efficiency transduction of

the GFP-pAAV-shFbxw7 vector was verified in C57BL/6 mice by immunofluorescence (Supplemental Figure 13A) and qRT-PCR (Supplemental Figure 13B). AAV-shFbxw7 treatment decreased mucosal ulcerations in *Il10^−/−* colitis mice (Figure 9, A and B). In the DSS-induced colitis model, AAV-shFbxw7–treated C57BL/6 mice had less of body weight loss, a lower DAI (Figure 9C), and an alleviated colon phenotype and shortening (Figure 9, D and E) when compared with AAV-shNC mice. Moreover, AAV-shFbxw7–treated mice showed significantly decreased expression of *Ccl2* and *Ccl7* in colon tissues, but significant change in expression of *Ccr2* and *Cx3cl1* (Figure 9F). Furthermore, AAV-shFbxw7 treatment significantly improved the survival of mice with colitis (Figure 9G) compared with AAV-shNC–treated mice. Altogether, these results suggest that AAV-mediated colonic *Fbxw7* silencing protects mice with colitis against inflammation and disease progression by downregulating *Ccl2* and *Ccl7* expression.

Discussion

The E3 ubiquitin ligase FBXW7 is mutated in approximately 10% of human colon cancers; it acts as a tumor suppressor in several tissues and targets multiple transcriptional activators and proto-oncogenes for ubiquitin-mediated degradation (41). However, the role of FBXW7 in inflammation and the immune response remains unknown. In this study, we revealed a mechanism for the mediation of IBD progression, whereby FBXW7 promotes *Ccl2* and *Ccl7*
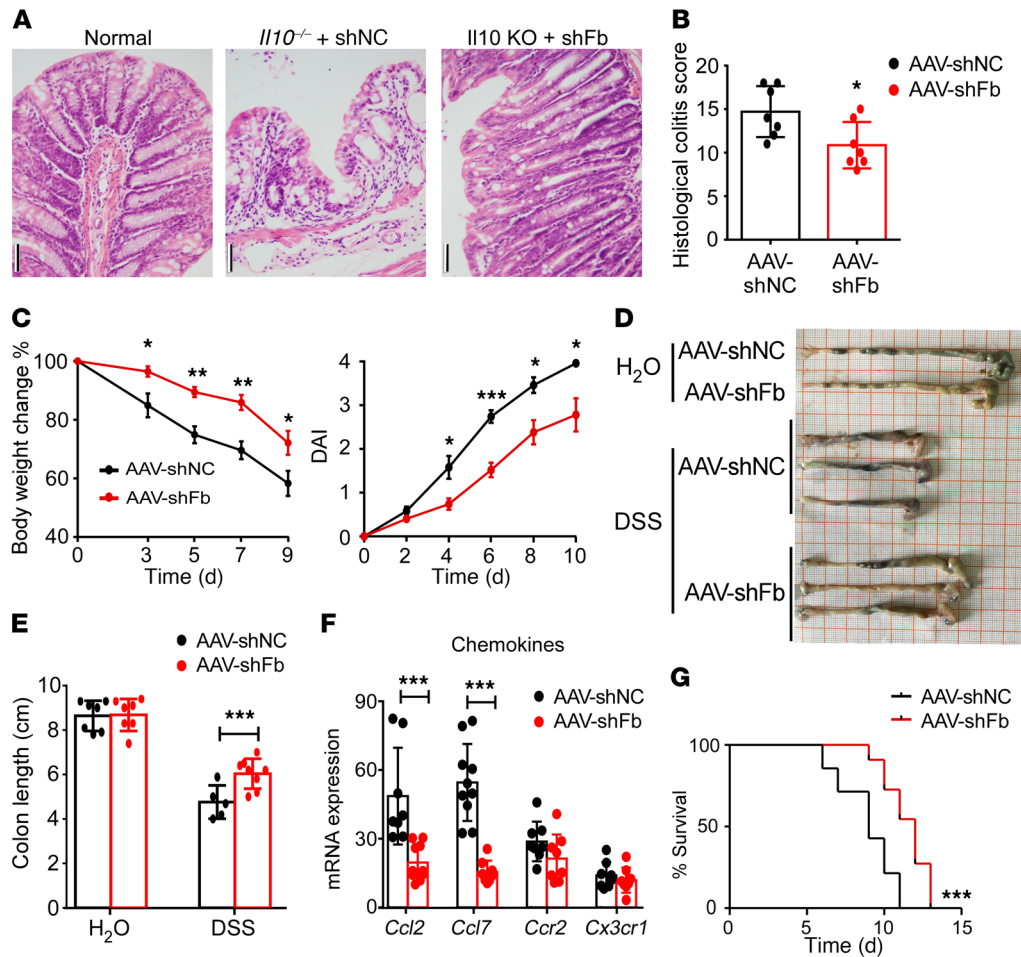
Figure 9. Decreased expression of *Fbxw7* relieves experimental colitis. (**A**) H&E-stained images of colon sections from 12-week-old *Il10*$^{-/-}$ mice injected with AAV weekly from 5 weeks until 9 weeks of age (*n* = 7) and their (**B**) histopathological colitis scores. Scale bars: 50 μm. (**C**) Body weight changes and DAI for healthy controls and C57BL/6 mice with DSS-induced colitis were assessed daily (*n* = 5). (**D**) Gross morphology of colons from healthy mice and mice with colitis sacrificed on day 9. (**E**) Colon length measurements (*n* = 7). (**F**) Colon tissue from mice sacrificed on day 7 was subjected to qRT-PCR to determine mRNA expression levels of chemokines and their ligands (*n* ≥6). Data are presented as the mean ± SD and are representative of at least 3 independent experiments. *$P < 0.05$, **$P < 0.01$, and ***$P < 0.001$, by unpaired, 2-tailed Student's *t* test (**B**, **C**, **E**, and **F**). (**G**) AAV-shNC– and AAV-shFB–treated mice were administered 4% DSS to induce acute colitis. Survival of mice was monitored until day 15 (*n* = 5). ***$P < 0.001$, by log-rank test. Data are representative of 3 independent experiments.

expression through the degradation of EZH2 in CX3CR1^{hi} resident macrophages, which results in increased recruitment of CX3CR1^{int} MPhs and amplification of intestinal inflammation. We believe our work provides new insights into the molecular and cellular networks of the intestinal inflammatory microenvironment.

A constant balance between resident macrophages and inflammatory MPhs is critical for maintaining homeostasis in a healthy gut and ensuring protective immunity when required. Interestingly, we noticed a more marked reduction of CD11b$^+$CX-3CR1^{hi} resident macrophages compared with CD11b$^+$CX3CR1^{int} inflammatory MPhs after liposome injection. This preferential ability may be due to the greater phagocytic activity of CD11b$^+$CX-3CR1^{hi} resident macrophages (42), which are key players in the capture and destruction of invading pathogens, as well as in the clearance of apoptotic or senescent cells. Our findings suggested that the increased susceptibility to DSS-induced colitis of both *Fbxw7*$^{fl/fl}$ and *LysM*$^+$ *Fbxw7*$^{fl/fl}$ mice after liposome treatment was related to the depletion of resident macrophages in the colon.

Furthermore, it is highly probable that the disappearance of the difference in colitis severity between *Fbxw7*$^{fl/fl}$ and *LysM*$^+$ *Fbxw7*$^{fl/fl}$ mice was due to the elimination of macrophages.

Altered profiles of inflammatory molecules and inflammation-related signaling pathways involving cytokines, chemokines, inflammasomes, antimicrobial peptides, and neuropeptides are all involved in the pathogenesis of CD and UC (3). The degree of local inflammation and tissue damage in UC and CD is dependent on the local expression of specific chemokines within IBD tissues. GWAS have pointed to several IBD susceptibility loci that contain genes that encode proteins involved in chemokine signaling, including CC-chemokine receptor 6 (*CCR6*), *CCL2*, and *CCL13*. A recent study has reported that treatment of intestinal crypts with supernatants of commensal-specific T cells from patients with CD induced higher protein secretion of the chemokines CXCL8 and CXCL1 and prompted a predominant neutrophil and Th17 recruitment to the intestinal epithelium (43). The expression of *Il17C* mRNA has been shown to correlate with *CCL20* in the inflamed

colon of patients with IBD (44). We found that upregulated *Fbxw7* in macrophages of the inflamed intestine promotes CCL2 and CCL7 production to facilitate the progression of colitis via the potent recruitment of proinflammatory MPhs. On the other hand, a protective role of *Fbxw7* in intestinal epithelium during acute intestinal inflammation has also been reported, as deletion of *Fbxw7* in the intestinal epithelium was found to promote DSS-induced colitis through activation of NF-κB signaling (45). This finding and our study revealed the differential function of *Fbxw7* in intestinal epithelium and myeloid cells within the intestinal microenvironment.

Recent studies have shown that, during inflammation, epigenetic mechanisms determine the unique tissue-specific identity and function of macrophages (46, 47). Trimethylation of H3K4 on cytokine gene promoters was shown to be induced in active M1 macrophages in response to TLR stimulation, leading to chromatin remodeling and inflammatory gene expression (48). IFN-dependent histone acetylation regulation instructs the development of the colitogenic monocyte and macrophage lineage in vivo during inflammation, suggesting a new insight into how macrophages gain colitogenic properties during the development of colitis (49). Demethylase KDM6A has been reported to promote transcription of the cytokines IL-6 and IFN-β in primary macrophages during the innate immune response through demethylation of H3K27me3 at the *Il6* and *Ifnb* promoters (50). A selective H3K27 demethylase inhibitor was also demonstrated to reduce LPS-induced proinflammatory cytokine production by human primary macrophages (51). EZH2, acting as a catalytic subunit of PRC2, is critical in mediating the formation of H3K27me3, which is associated with transcriptional gene suppression (34). Ezh2 deficiency has been shown to affect TNF-α signaling and promote the inflammatory response in intestinal epithelial cells in colitis (52). We provide evidence that threonine at positions 261 and 367 of EZH2 is essential for the interaction of EZH2 with FBXW7 and that this interaction mediates the function of FBXW7 in reducing EZH2 expression in resident macrophages upon DSS challenge. The relationship between FBXW7 and epigenetic modifiers has been reported in tumorigenesis (53), but it remains largely unknown in inflammation. Here, we have demonstrated that expression of CCL2 and CCL7 produced by resident macrophages from *LysM*+ *Fbxw7*fl/fl mice was lower than that in macrophages from *Fbxw7*fl/fl littermates and that a selective inhibitor of H3K27me3 in macrophages had the effect of promoting *Ccl2* and *Ccl7* expression.

In summary, we identified a critical role of FBXW7 in the regulation of colitis by inducing *Ccl2* and *Ccl7* expression in resident macrophages and promoting the accumulation of proinflammatory MPhs. FBXW7/EZH2/CCL2/CCL7 is an important pathway for shaping the status and activity of colon-resident macrophages and inflammatory MPhs in the colitis setting. Our results indicate that FBXW7 may be a predictive marker of IBD severity and a potential target for IBD treatment, since *Fbxw7* siRNA had a significant therapeutic effect in our colitis mouse model.

Methods

Mice and reagents. *Fbxw7*fl/fl mice (on a C57BL/6J background) were obtained from The Jackson Laboratory. *LysM-Cre* mice on a C57BL/6J background were provided by Ximei Wu (Zhejiang University School of Medicine, Hangzhou, China). *Il10*−/− mice were provided by Yanmei

Han (National Key Laboratory of Medical Immunology and Institute of Immunology, Second Military Medical University, Shanghai, China). All mice were bred at the Zhejiang University Laboratory Animal Center under specific pathogen–free conditions. C57BL/6 mice were purchased from the Model Animal Research Center of Nanjing University (Nanjing, China).

Mice were born and bred at the same facility and kept on the same rack in an animal housing room that was maintained under specific pathogen–free conditions with a controlled temperature (22°C) and photoperiod (12-hour light/12-hour dark cycle) and unrestricted access to standard mouse chow and water, except for mice used in some experiments described herein. The cohousing experiments were conducted with weaned 3-week-old *Fbxw7*fl/fl mice that were randomly cohoused with age-matched *LysM*+ *Fbxw7*fl/fl mice at a 1:1 ratio for 7 weeks prior to DSS colitis induction, which was performed during the cohousing period.

Abs against the HA tag (sc-805), Myc tag (sc-40; sc-789), Flag tag (sc-807), GAPDH (sc-130619), and ubiquitin (sc-271289) were obtained from Santa Cruz Biotechnology. Abs specific for p-p65 (product no. 3033), p65 (product no. 8242), EZH2 (product no. 3147), and HIF-1α (product no. 36169) were from Cell Signaling Technology. Lys48-specific linked polyubiquitin Ab (product no. 05-1307) was from MilliporeSigma. Abs against FBXW7 were obtained from Abcam (ab12292) and Thermo Fisher Scientific (40-1500). Abs against H3K36me3 (ab9050), H3K9me3 (ab8898), H3K4me3 (ab8580), H3K27me3 (ab6002), and H3 (ab1791) were from purchased from Abcam. MG132 (M8699), CHX (C4859), and Flag-M2 Magnetic Beads (product no. M8823) were from MilliporeSigma. ELISA kits for mouse IL-6 (BMS603-2), TNF-α (BMS607-3), CCL2 (BMS6005), and CCL7 (BMS6006INST) were purchased from eBioscience.

Human peripheral blood samples. A total of 68 peripheral blood samples were collected from patients with IBD hospitalized in Sir Run Run Shaw Hospital (Zhejiang University School of Medicine, China) from May 11, 2017 to August 1, 2017, and from 50 healthy adults as a control group. The diagnosis and IBD severity evaluation were made according to the 2012 Expert Consensus Document on the Diagnosis and Treatment of IBD formulated by the Chinese Society for Gastroenterology (CSGE) (54). The severity of CD was determined using the Best CD activity index (CDAI) calculator (55). The severity of UC disease was determined by the Mayo Score with composite indices (56). Basic information concerning the patients, including age and sex, is summarized in Supplemental Table 1. Monocytes were isolated using a human monocyte isolation kit (Haoyang Biological Technology Co.) according to the manufacturer's recommendations.

Randomization method. The following covariates for mice were controlled: age, sex, littermate status, and age (8–10 weeks). Adult male mice and their littermates were used. Under such conditions, the mice were randomly assigned to experimental groups. For studies using media collected from stimulated cells or tissues, samples were randomly allocated to ELISA plate wells prior to measurement. Random fields were analyzed in confocal H&E-stained and immunohistochemical images.

Fecal microbiome analysis. *LysM*+ *Fbxw7*fl/fl mice and *Fbxw7*fl/fl littermates (8- to 10-week-old male or female C57BL/6J mice) were fed in different cages. The mice were kept in the same environment with the other experimental mice. Freshly formed feces were collected from the cage and weighed. Bacterial DNA was extracted from the stool

using a QIAamp Fast DNA Stool Mini Kit (QIAGEN). DNA concentration and purity were monitored on 1% agarose gels, after which DNA was diluted to 1 ng/μL using sterile water.

Amplicon generation, PCR products mixing and purification, library preparation, and sequencing of the 16S rDNA gene were performed by Novogene Bioinformatics Technology to determine bacterial composition and diversity, using IonS5 XL 16S rDNA amplicon sequencing. Sequencing libraries were generated using a 48-Reaction Ion Plus Fragment Library Kit (Thermo Fisher Scientific) following the manufacturer's recommendations. Data analysis was also conducted by Novogene Bioinformatics Technology according to the previous literature (57, 58). Statistical analysis of sequencing data was performed using UPARSE software, version 7.0.100 (http://drive5.com/uparse/) (59). Sequences with 97% or greater similarity were assigned to the same OTUs.

Cell culture. HEK293T cells (American Type Culture Collection [ATCC], CRL-11268) were maintained in DMEM medium, and thioglycolate-elicited mouse peritoneal macrophages (BD, 3190383; Merck, 1.08191.0500) were cultured in RPMI 1640 medium with 10% (vol/vol) FCS. BMDMs were generated using BM from femurs and tibiae of 6- to 8-week-old mice (25).

Induction of colitis. Eight- to ten-week-old *LysM⁺ Fbxw7ᶠˡ/ᶠˡ* C57BL/6 mice and *Fbxw7ᶠˡ/ᶠˡ* littermates were studied using TNBS or DSS-induced colitis models as described previously (60). Mice were treated with 3% DSS (MP Biomedical) in the drinking water (w/v) for 7 days, followed by 2 days of regular drinking water before sacrifice. In the recovery experiment, *LysM⁺ Fbxw7ᶠˡ/ᶠˡ* mice and *Fbxw7ᶠˡ/ᶠˡ* littermates were treated with DSS for 7 days, followed by a 13-day recovery period, and control mice were treated with water. In the survival experiment, the mice were given 4% DSS in the drinking water for 7 days, followed by regular drinking water until the end of the study.

Overnight-fasted mice were intrarectally injected with 100 mg/kg TNBS (MilliporeSigma) in 50% ethanol, with 50% ethanol treatment used as a control. The *LysM⁺ Fbxw7ᶠˡ/ᶠˡ* mice and *Fbxw7ᶠˡ/ᶠˡ* littermates were sacrificed 5 days after TNBS treatment.

Il10⁻/⁻ mice spontaneously developed chronic IBD under specific pathogen–free conditions in our animal facility. The phenotypes of chronic enterocolitis were more evident when *Il10⁻/⁻* mice were 12 weeks of age or older.

Analysis of colon explant cultures and ELISA. The colons of mice were flushed with PBS containing 30% antibiotics, and open along a longitudinal axis. Then, pieces of tissue (~ 3-mm²) were obtained from the distal colon and incubated for 24 hours in RPMI supplemented with 10% FCS and 20% antibiotics (1 punch biopsy/100 mL medium). Supernatants were collected and kept frozen until assessment. CCL2 and CCL7 levels in the supernatant were detected by conventional double-sandwich ELISA (BD Biosciences).

Flow cytometry. The following fluorochrome-labeled mAbs and staining reagents were used according to the manufacturers' protocols: lamina propria cells were stained with anti–CD11b-FITC (BioLegend, 101217), anti–Ly6C-FITC (BioLegend, 128005), anti–Gr-1-FITC (BioLegend, 108417), anti–CD11b-PE (BioLegend, 101208), anti–CX3CR1-PE (BioLegend, 149006), anti–CD11C-APC (BioLegend, 117310), anti–F4/80-FITC (BioLegend, 123120), anti–Ly6G-FITC (BioLegend, 127605), anti–CD45.2-APC (eBioscience, 104), anti–Ly6C-percp cy5.5 and a Zombie Violet Fixable Viability Kit (BioLegend, 423114), anti–F4/80-CF594 (BioLegend, 123131), anti–CD103-BV605 (BD, 740355), anti–EZH2-FITC (BD, 562479), and anti–human Cdc4 (Thermo Fisher Scientific,

40-1500). The cells were analyzed with a NovoCyte Flow Cytometer (ACEA) or a BD Fortessa, or were sorted with a BD FACSAria machine. Flow cytometric analysis was performed using FlowJo software.

Gene expression analysis. Total RNA was extracted from cells using TRIzol Reagent (Takara) according to the manufacturer's directions. Subsequently, single-strand cDNA synthesis was performed using a Tyobo reverse transcription kit. For the DSS-induced colitis model, RNA reverse transcription was performed as previously described (61). Total cDNA from macrophages and monocytes sorted from mouse colons was extracted using a Single Cell Sequence Specific Amplification Kit (Vazyme). qRT-PCR was performed using SYBR Green Master Rox (Roche) on a CFX-96 (Bio-Rad) or 480II (Roche) Real-Time PCR System, and *Actb* was used as a housekeeping gene. The primer sequences are listed in Supplemental Table 2.

Monocyte transfer experiment. Briefly, mice received a sublethal dose of γ ray irradiation (8 Gy) to induce BM cell damage on day 3 or 7 after DSS challenge. Six hours after irradiation, *LysM⁺ Fbxw7ᶠˡ/ᶠˡ* (KO) mice and *Fbxw7ᶠˡ/ᶠˡ* littermate (WT) mice received 100 μL fresh WT and KO mixed monocytes labeled with cell proliferation Dye eFluor 450 (eBioscience, 65-0842-90) and eFluor 670 (eBioscience, 65-0840-85) at a concentration of 1 × 10⁷/mL, respectively (WT plus KO→WT and WT plus KO→KO groups). Ly6Cʰⁱ monocytes were sorted to high purity (>95%), and 1 day after monocyte transfer, CLP from mice was collected and analyzed by flow cytometry.

Migration assay. Sorted splenic Ly6Cʰⁱ monocytes (1 × 10⁴) from *Fbxw7ᶠˡ/ᶠˡ* and *LysM⁺ Fbxw7ᶠˡ/ᶠˡ* mice were added into the upper compartment of the Transwell chambers (24-well plates, 8-mm pores, BD Biosciences) in 100 μL serum-free medium. Sorted CX3CR1ʰⁱ resident or CX3CR1ⁱⁿᵗ proinflammatory MPhs (5 × 10⁵) from CLP of *Fbxw7ᶠˡ/ᶠˡ* mice or *LysM⁺ Fbxw7ᶠˡ/ᶠˡ* mice with colitis were cultured in 600 μL RPMI 1640 serum-free medium. After 24 hours, the culture supernatant was harvested and added into the lower chamber of the Transwell plate as a chemotactic stimulus. In some conditions, CCL2 (R&D Systems, AF-479-NA) and CCL7 (R&D Systems, AF-456-NA) Abs were added to the conditioned medium in the lower chamber 2 hours before incubation. After a 24-hour inoculation at 5% CO₂ and 37°C, the cells that had dropped into the lower chamber were counted by cytometry, and cells that clung to the bottom side of the polycarbonate membrane were fixed with 10% formalin and stained with DAPI.

For the in vivo migration assay, every 48 hours on days –1, 1, 3, and 5 during DSS treatment, mice were i.p. injected with anti-CCL2 and anti-CCL7 Abs (R&D Systems, AF-479-NA and AF-456-NA) or a rat IgG2a isotype control mAb (BioLegend, RTK2758) diluted in sterile PBS.

Phagocytosis assay. Fluorescein conjugate *E. coli* (K-12 strain) BioParticles (Molecular Probes, E2861, FITC-labeled heat-killed *E. coli*) were diluted in serum media and incubated for 30 minutes, followed by 2 washes in PBS. Next, FITC-labeled, heat-killed *E. coli* was added to RPMI-1640 medium with 10% FCS and incubated with cells for 1 hour in a humidified atmosphere of 5% CO₂ at 4°C or 37°C, and cells were washed twice with PBS before trypsinization and then washed once with trypan blue, followed by flow cytometric analysis.

Depletion of macrophages. Macrophages were depleted using CLs (ClodronateLiposomes.org) as described previously (62). In brief, mice were anesthetized, and CLs were injected via the tail vein (100 μL) and i.p. (100 μL) into mice on days –1, 1, 3, and 5 during DSS treatment. Liposome-encapsulated PBS was not used as a negative control, because the uptake of these liposomes by colonic macrophages was

shown to result in a partial reduction of macrophages (63). Controls included i.p. injections of 200 μL PBS.

Preparation of mouse neutrophils from peripheral blood. Mouse blood (350 ± 50 μL per animal) was collected by tail bleeding into HBSS-EDTA (HBSS without calcium, magnesium, phenol red, and sodium bicarbonate; pH 7.2, 15 mM EDTA, BSA, 1%). Neutrophils were isolated using Percoll-based density gradient centrifugation (64) (350,000 ± 40,000 cells were obtained per mouse, 97% of which were neutrophils).

Neutrophil depletion. Every 48 hours on days –1, 1, 3, and 5 during DSS treatment, mice were i.p. injected with 400 μg anti-Ly6G mAb (BioLegend, 1A8) or rat IgG2a isotype control mAb (BioLegend, RTK2758) diluted in sterile PBS. For confirmation of depletion during the colitis experiments, colons from anti-Ly6G–treated and isotype control–treated mice in health or with colitis were harvested for each independent experiment and analyzed by flow cytometry for a reduction in CD45+CD11b+Gr-1+ cells.

Immunohistochemical and immunofluorescence staining. Colon tissues were fixed in 4% formalin, and immunohistochemical and immunofluorescence staining was performed for human and mouse colon sections at the Histomorphology Platform of Zhejiang University, following the manufacturer's standard protocol (reagents purchased from Beijing Zhongshan Jinqiao Biotechnology Company). Human colon specimens were scored using Constantine's protocol (65), under high magnification, and integrated staining intensity and the percentage of positive cells were scored.

Colitis analysis. Colons were collected immediately after the mice were sacrificed. The entire colon (from the cecum to the anus) was removed and measured, and colon lengths were reported as described previously (66). The distal colon was removed, fixed in 10% formalin, and the tissue sections were paraffin embedded and stained with H&E for light microscopic examination to assess colon injury and inflammation. The degree of colitis was scored without any prior knowledge of the experimental groups as follows (67): degree of epithelial regeneration (scale of 0–3), distortion/branching (scale of 0–3), inflammation (scale of 0–3) and crypt damage (scale of 0–4), percentage of area with inflammation (scale of 0–4) and crypt damage (scale of 0–4), and depth of inflammation (scale of 0–3) . The total score ranged from 0 points (no colitis) to 24 points (severe colitis).

In TNBS-induced colitis, the DAI (scale of 0 to 4) was monitored daily and used to assess the severity of colitis on the basis of weight loss, blood in the stool, and stool consistency according to described previously methods (68).

Plasmid constructs and transfection. Recombinant vectors encoding mouse *Ezh2* were created by PCR-based amplification of complementary DNA from murine BM cells, followed by subcloning into the Pcmv-Tag2B eukaryotic expression vector (Invitrogen, Thermo Fisher Scientific). All constructs were confirmed by DNA sequencing. The plasmids were transfected into HEK293T cells with JetPrime (Polyplus). Primary macrophages were transfected with siRNA through the use of INTERFERin Reagent (Polyplus) according to the standard protocol. BMDMs were transfected with siRNA using INTERFERin Reagent (Polyplus) according to the standard protocol. The *Ezh2* siRNA sequences were 5′-GCACAAGTCATCCCGTTAA-3′, 5′-GCAACAC-CCAACACATATA-3′, and 5′-GCAAATTCTCGGTGTCAAA-3′ (Gene Pharma). *Fbxw7* siRNA sequences were 5′-ACCTTCTCTGGAGA-GAGAAATGC-3′, 5′-GTGTGGAATGCTGAAACTGGAGA-3′, and

5′-CACAAAGCTGGTGTGTGCA-3′ (Life Technologies, Thermo Fisher Scientific).

Immunoprecipitation and immunoblot analyses. SDS-PAGE and immunoblot analysis were performed as described previously (25). BMDMs were immunoprecipitated using anti-FBXW7 plus protein A/G agarose. The proteins were then separated using SDS-PAGE and subjected to immunoblot analysis with anti-EZH2 or anti-FBXW7 Abs.

ChIP analysis. ChIP analysis was done using H3K27me3 (Abcam, ab6002), as described previously (69), and the process was performed according to the manufacturer's instructions for the ChIP Assay Kit (Cell Signaling Technology). Fold enrichment was quantified using qRT-PCR and calculated as a percentage of input chromatin (percentage of input).

RNA-Seq. Total RNA from BMDMs ($1 × 10^6$) was extracted using TRIzol (Takara). Preparation of the library and transcriptomic sequencing were carried out using the Illumina HiSeq ×Ten (Novogene Bioinformatics Technology). Mapping of 100-bp paired-end reads to genes was done using HTSeq software (version 0.6.0), and fragments per kilobase of transcript per million fragments mapped (FPKM) were also analyzed. RNA-Seq data are available in the NCBI's Gene Expression Omnibus (GEO) repository (GEO GSE125242).

pAAV-EGFP administration. Mice were fasted overnight and pretreated with 20 mM *N*-acetyl-L-cysteine (NAC) (MilliporeSigma) as described previously (70) and then anesthetized with chloral hydrate by i.p. injection. The colon was washed with an intrarectal injection of 100 μL of 20 mM NAC using a stainless-steel straight, round-tipped microsyringe and allowed to drain for 15 minutes, and this step was repeated twice. Next, mice were reanesthetized, and $5 × 10^{10}$ physical particles of pAAV-EGFP in 100 μL PBS were administered by enema, and tail-vein injection of pAAV-EGFP was given once a week for 3 weeks. The transgene plasmids used were p-AAV-CMV-EGFP and p-AAV-shFbxw7 (U6-shNC/shFbxw7-mir30arm) and were generated by Shanghai SunBio Medical Biotechnology.

Statistics. Statistical analysis was performed with GraphPad Prism software. All data are expressed as the mean ± SEM or SD. All experiments were repeated independently at least 3 times. Statistical significance between 2 experimental groups was determined using an unpaired, 2-tailed Student's *t* test. Differences with a *P* value of less than 0.05 were considered statistically significant. Three or more groups were compared with ANOVA. Multiple comparisons between variables were assessed by 1-way ANOVA with Tukey's multiple comparisons test. For the mouse survival study, Kaplan-Meier survival curves were generated, and a log-rank test (Mantel-Cox) was used to determine statistical significance.

Study approval. Written patient consent was provided, and ethics approval for the use of human samples was granted by the Medical Ethics Committee of Zhejiang University School of Medicine before harvesting of human tissue and blood samples. All animal research was performed under a protocol approved by the Medical Experimental Animal Care Commission of Zhejiang University.

Author contributions

QW, LL, and JH designed the research. JH, YS, GL, YL, YX, XT, TP, ZJ, and LL performed experiments and acquired and analyzed data. PX and QC provided clinical specimens. JH, LL, and QW wrote the manuscript. XC supervised the study. All authors read and approved the final manuscript.

Acknowledgments

Address correspondence to: Qingqing Wang or Lihua Lai, Institute of Immunology, Zhejiang University School of Medicine, 866 Yu Hang Tang Road, Hangzhou 310058, Zhejiang, China. Phone: 86.571.88208284; Email: wqq@zju.edu.cn, lailihua@zju.edu.cn.

1. de Souza HS, Fiocchi C. Immunopathogenesis of IBD: current state of the art. *Nat Rev Gastroenterol Hepatol*. 2016;13(1):13–27.

2. Kostic AD, Xavier RJ, Gevers D. The microbiome in inflammatory bowel disease: current status and the future ahead. *Gastroenterology*. 2014;146(6):1489–1499.

3. Neurath MF. Cytokines in inflammatory bowel disease. *Nat Rev Immunol*. 2014;14(5):329–342.

4. Bain CC, Schridde A. Origin, Differentiation, and Function of Intestinal Macrophages. *Front Immunol*. 2018;9:2733.

5. Mosser DM, Edwards JP. Exploring the full spectrum of macrophage activation. *Nat Rev Immunol*. 2008;8(12):958–969.

6. Strober W, Fuss IJ. Proinflammatory cytokines in the pathogenesis of inflammatory bowel diseases. *Gastroenterology*. 2011;140(6):1756–1767.

7. Bain CC, et al. Resident and pro-inflammatory macrophages in the colon represent alternative context-dependent fates of the same Ly6Chi monocyte precursors. *Mucosal Immunol*. 2013;6(3):498–510.

8. Joeris T, Müller-Luda K, Agace WW, Mowat AM. Diversity and functions of intestinal mononuclear phagocytes. *Mucosal Immunol*. 2017;10(4):845–864.

9. Smythies LE, et al. Human intestinal macrophages display profound inflammatory anergy despite avid phagocytic and bacteriocidal activity. *J Clin Invest*. 2005;115(1):66–75.

10. Zigmond E, et al. Ly6C hi monocytes in the inflamed colon give rise to proinflammatory effector cells and migratory antigen-presenting cells. *Immunity*. 2012;37(6):1076–1090.

11. Grainger JR, Konkel JE, Zangerle-Murray T, Shaw TN. Macrophages in gastrointestinal homeostasis and inflammation. *Pflugers Arch*. 2017;469(3-4):527–539.

12. Bain CC, Mowat AM. Macrophages in intestinal homeostasis and inflammation. *Immunol Rev*. 2014;260(1):102–117.

13. Zigmond E, Jung S. Intestinal macrophages: well educated exceptions from the rule. *Trends Immunol*. 2013;34(4):162–168.

14. Asano K, et al. Intestinal CD169(+) macrophages initiate mucosal inflammation by secreting CCL8 that recruits inflammatory monocytes. *Nat Commun*. 2015;6:7802.

15. Lieber S, et al. Prognosis of ovarian cancer is associated with effector memory CD8+ T cell accumulation in ascites, CXCL9 levels and activation-triggered signal transduction in T cells. *Oncoimmunology*. 2018;7(5):e1424672.

16. Wunderlich CM, et al. Obesity exacerbates colitis-associated cancer via IL-6-regulated macrophage polarisation and CCL-20/CCR-6-mediated lymphocyte recruitment. *Nat Commun*. 2018;9(1):1646.

17. Gaujoux R, et al. Cell-centred meta-analysis reveals baseline predictors of anti-TNFα non-response in biopsy and blood of patients with IBD. *Gut*. 2019;68(4):604–614.

18. Kochumon S, et al. Palmitate Activates CCL4 Expression in Human Monocytic Cells via TLR4/MyD88 Dependent Activation of NF-κB/MAPK/PI3K Signaling Systems. *Cell Physiol Biochem*. 2018;46(3):953–964.

19. Sans M, et al. Enhanced recruitment of CX3CR1+ T cells by mucosal endothelial cell-derived fractalkine in inflammatory bowel disease. *Gastroenterology*. 2007;132(1):139–153.

20. Taki M, et al. Snail promotes ovarian cancer progression by recruiting myeloid-derived suppressor cells via CXCR2 ligand upregulation. *Nat Commun*. 2018;9(1):1685.

21. Welcker M, Clurman BE. FBW7 ubiquitin ligase: a tumour suppressor at the crossroads of cell division, growth and differentiation. *Nat Rev Cancer*. 2008;8(2):83–93.

22. Onoyama I, et al. Fbxw7 regulates lipid metabolism and cell fate decisions in the mouse liver. *J Clin Invest*. 2011;121(1):342–354.

23. Yumimoto K, Matsumoto M, Onoyama I, Imaizumi K, Nakayama KI. F-box and WD repeat domain-containing-7 (Fbxw7) protein targets endoplasmic reticulum-anchored osteogenic and chondrogenic transcriptional factors for degradation. *J Biol Chem*. 2013;288(40):28488–28502.

24. Ekholm-Reed S, Goldberg MS, Schlossmacher MG, Reed SI. Parkin-dependent degradation of the F-box protein Fbw7β promotes neuronal survival in response to oxidative stress by stabilizing Mcl-1. *Mol Cell Biol*. 2013;33(18):3627–3643.

25. Song Y, et al. E3 ligase FBXW7 is critical for RIG-I stabilization during antiviral responses. *Nat Commun*. 2017;8:14654.

26. Arranz A, et al. Akt1 and Akt2 protein kinases differentially contribute to macrophage polarization. *Proc Natl Acad Sci U S A*. 2012;109(24):9517–9522.

27. Nishikawa K, et al. Interleukin-17 induces an atypical M2-like macrophage subpopulation that regulates intestinal inflammation. *PLoS ONE*. 2014;9(9):e108494.

28. Geissmann F, Manz MG, Jung S, Sieweke MH, Merad M, Ley K. Development of monocytes, macrophages, and dendritic cells. *Science*. 2010;327(5966):656–661.

29. Banks C, Bateman A, Payne R, Johnson P, Sheron N. Chemokine expression in IBD. Mucosal chemokine expression is unselectively increased in both ulcerative colitis and Crohn's disease. *J Pathol*. 2003;199(1):28–35.

30. Platt AM, Bain CC, Bordon Y, Sester DP, Mowat AM. An independent subset of TLR expressing CCR2-dependent macrophages promotes colonic inflammation. *J Immunol*. 2010;184(12):6843–6854.

31. Serbina NV, Pamer EG. Monocyte emigration from bone marrow during bacterial infection requires signals mediated by chemokine receptor CCR2. *Nat Immunol*. 2006;7(3):311–317.

32. Hoesel B, Schmid JA. The complexity of NF-κB signaling in inflammation and cancer. *Mol Cancer*. 2013;12:86.

33. Storti P, et al. Hypoxia-inducible factor (HIF)-1α suppression in myeloma cells blocks tumoral growth in vivo inhibiting angiogenesis and bone destruction. *Leukemia*. 2013;27(8):1697–1706.

34. McCabe MT, et al. Mutation of A677 in histone methyltransferase EZH2 in human B-cell lymphoma promotes hypertrimethylation of histone H3 on lysine 27 (H3K27). *Proc Natl Acad Sci U S A*. 2012;109(8):2989–2994.

35. Bai C, et al. SKP1 connects cell cycle regulators to the ubiquitin proteolysis machinery through a novel motif, the F-box. *Cell*. 1996;86(2):263–274.

36. Hoeck JD, et al. Fbw7 controls neural stem cell differentiation and progenitor apoptosis via Notch and c-Jun. *Nat Neurosci*. 2010;13(11):1365–1372.

37. Welcker M, et al. The Fbw7 tumor suppressor regulates glycogen synthase kinase 3 phosphorylation-dependent c-Myc protein degradation. *Proc Natl Acad Sci U S A*. 2004;101(24):9085–9090.

38. Zhang W, Koepp DM. Fbw7 isoform interaction contributes to cyclin E proteolysis. *Mol Cancer Res*. 2006;4(12):935–943.

39. Nguyen KD, Fentress SJ, Qiu Y, Yun K, Cox JS, Chawla A. Circadian gene Bmal1 regulates diurnal oscillations of Ly6C(hi) inflammatory monocytes. *Science*. 2013;341(6153):1483–1488.

40. McCabe MT, et al. EZH2 inhibition as a therapeutic strategy for lymphoma with EZH2-activating mutations. *Nature*. 2012;492(7427):108–112.

41. Babaei-Jadidi R, et al. FBXW7 influences murine intestinal homeostasis and cancer, targeting Notch, Jun, and DEK for degradation. *J Exp Med*. 2011;208(2):295–312.

42. A-Gonzalez N, et al. Phagocytosis imprints heterogeneity in tissue-resident macrophages. *J Exp Med*. 2017;214(5):1281–1296.

43. Calderón-Gómez E, et al. Commensal-specific CD4(+) cells from patients with Crohn's disease have a T-helper 17 inflammatory profile. *Gastroenterology*. 2016;151(3):489–500.e3.

44. Friedrich M, Diegelmann J, Schauber J, Auernhammer CJ, Brand S. Intestinal neuroendocrine cells and goblet cells are mediators of IL-17A-amplified epithelial IL-17C production in human inflammatory bowel disease. *Mucosal Immunol*. 2015;8(4):943–958.

45. Li H, Liang Y, Lai X, Wang W, Zhang J, Chen S. Genetic deletion of Fbw7 in the mouse intestinal epithelium aggravated dextran sodium sulfate-induced colitis by modulating the inflammatory response of NF-κB pathway. *Biochem Biophys Res Commun*. 2018;498(4):869–876.

46. Amit I, Winter DR, Jung S. The role of the local environment and epigenetics in shaping macro-

phage identity and their effect on tissue homeostasis. *Nat Immunol*. 2016;17(1):18–25.

47. Ventham NT, Kennedy NA, Nimmo ER, Satsangi J. Beyond gene discovery in inflammatory bowel disease: the emerging role of epigenetics. *Gastroenterology*. 2013;145(2):293–308.

48. Takeuch O, Akira S. Epigenetic control of macrophage polarization. *Eur J Immunol*. 2011;41(9):2490–2493.

49. Nakanishi Y, Sato T, Takahashi K, Ohteki T. IFN-γ–dependent epigenetic regulation instructs colitogenic monocyte/macrophage lineage differentiation in vivo. *Mucosal Immunol*. 2018;11(3):871–880.

50. Li X, et al. Demethylase Kdm6a epigenetically promotes IL-6 and IFN-β production in macrophages. *J Autoimmun*. 2017;80:85–94.

51. Kruidenier L, et al. A selective jumonji H3K27 demethylase inhibitor modulates the proinflammatory macrophage response. *Nature*. 2012;488(7411):404–408.

52. Liu Y, et al. Epithelial EZH2 serves as an epigenetic determinant in experimental colitis by inhibiting TNFα-mediated inflammation and apoptosis. *Proc Natl Acad Sci U S A*. 2017;114(19):E3796–E3805.

53. Zhao E, et al. Cancer mediates effector T cell dysfunction by targeting microRNAs and EZH2 via glycolysis restriction. *Nat Immunol*. 2016;17(1):95–103.

54. Chinese Society of Gastroenterology. Expert Consensus for the Diagnosis and Treatment of Inflammatory Bowel Disease [in Chinese]. *Chinese Journal of Internal Medicine*. 2012;51(10):818–831.

55. Best WR, Becktel JM, Singleton JW, Kern F. Development of a Crohn's disease activity index. National Cooperative Crohn's Disease Study. *Gastroenterology*. 1976;70(3):439–444.

56. Levesque BG, Sandborn WJ, Ruel J, Feagan BG, Sands BE, Colombel JF. Converging goals of treatment of inflammatory bowel disease from clinical trials and practice. *Gastroenterology*. 2015;148(1):37–51.e1.

57. Edgar RC, Haas BJ, Clemente JC, Quince C, Knight R. UCHIME improves sensitivity and speed of chimera detection. *Bioinformatics*. 2011;27(16):2194–2200.

58. Haas BJ, et al. Chimeric 16S rRNA sequence formation and detection in Sanger and 454-pyrosequenced PCR amplicons. *Genome Res*. 2011;21(3):494–504.

59. Edgar RC. UPARSE: highly accurate OTU sequences from microbial amplicon reads. *Nat Methods*. 2013;10(10):996–998.

60. Wirtz S, Neufert C, Weigmann B, Neurath MF. Chemically induced mouse models of intestinal inflammation. *Nat Protoc*. 2007;2(3):541–546.

61. Bosma M, et al. FNDC4 acts as an anti-inflammatory factor on macrophages and improves colitis in mice. *Nat Commun*. 2016;7:11314.

62. Qualls JE, Kaplan AM, van Rooijen N, Cohen DA. Suppression of experimental colitis by intestinal mononuclear phagocytes. *J Leukoc Biol*. 2006;80(4):802–815.

63. Bradley PP, Priebat DA, Christensen RD, Rothstein G. Measurement of cutaneous inflammation: estimation of neutrophil content with an enzyme marker. *J Invest Dermatol*. 1982;78(3):206–209.

64. Boxio R, Bossenmeyer-Pourié C, Steinckwich N, Dournon C, Nüsse O. Mouse bone marrow contains large numbers of functionally competent neutrophils. *J Leukoc Biol*. 2004;75(4):604–611.

65. Constantine CE, Wreghitt TG. A rapid microagglutination technique for the detection of antibody to *Legionella pneumophila* serogroup 5. *J Med Microbiol*. 1991;34(1):29–31.

66. Okayasu I, Hatakeyama S, Yamada M, Ohkusa T, Inagaki Y, Nakaya R. A novel method in the induction of reliable experimental acute and chronic ulcerative colitis in mice. *Gastroenterology*. 1990;98(3):694–702.

67. Fukata M, et al. Toll-like receptor-4 promotes the development of colitis-associated colorectal tumors. *Gastroenterology*. 2007;133(6):1869–1881.

68. Lin W, et al. Raf kinase inhibitor protein mediates intestinal epithelial cell apoptosis and promotes IBDs in humans and mice. *Gut*. 2017;66(4):597–610.

69. Chen K, et al. Methyltransferase SETD2-mediated methylation of STAT1 is critical for interferon antiviral activity. *Cell*. 2017;170(3):492–506.e14.

70. Polyak S, et al. Identification of adeno-associated viral vectors suitable for intestinal gene delivery and modulation of experimental colitis. *Am J Physiol Gastrointest Liver Physiol*. 2012;302(3):G296–G308.